frontiers | Frontiers in Environmental Chemistry

ORIGINAL RESEARCH
published: 22 June 2022
doi: 10.3389/fenvc.2022.803944

Neodymium Isotopic Composition and Rare Earth Element Concentration Variations in the Coral and Solomon Seas

Viet Quoc Pham [1,2], Catherine Jeandel [1]*, Melanie Grenier [1], Sophie Cravatte [1], Gerard Eldin [1], Moustafa Belhadj [1], Cyril Germineaud [3] and Tu Van Vu [2]*

[1]LEGOS, Université de Toulouse, (CNRS, UPS, IRD, CNES), Toulouse, France, [2]Institute of Environmental Technology, Vietnam Academy of Science and Technology, Hanoi, Vietnam, [3]Mercator Ocean International, Toulouse, France

OPEN ACCESS

Edited by:
David Amouroux, UMR5254 Institut des Sciences Analytiques et de Physico-Chimie pour l'Environnement et les Matériaux (IPREM), France

Reviewed by:
Torben Stichel, Alfred Wegener Institute Helmholtz Centre for Polar and Marine Research (AWI), Germany
April N. Abbott, Coastal Carolina University, United States

***Correspondence:**
Catherine Jeandel
catherine.jeandel@legos.obs-mip.fr
Viet Quoc Pham
vietpq@ietvn.vn

Specialty section:
This article was submitted to Inorganic Pollutants, a section of the journal Frontiers in Environmental Chemistry

Received: *28 October 2021*
Accepted: *05 May 2022*
Published: *22 June 2022*

Citation:
Pham VQ, Jeandel C, Grenier M, Cravatte S, Eldin G, Belhadj M, Germineaud C and Vu TV (2022) Neodymium Isotopic Composition and Rare Earth Element Concentration Variations in the Coral and Solomon Seas. Front. Environ. Chem. 3:803944. doi: 10.3389/fenvc.2022.803944

Significant progress has been made in the last decade on the understanding of the role of the Coral and Solomon Seas as major suppliers of waters and chemical elements to the equatorial Pacific. Yet, the location, depth, and processes of chemical enrichment of these waters remain poorly constrained. Neodymium (Nd) isotopic compositions (ε_{Nd}) and rare earth element concentrations (REE) are powerful tracers of land-ocean chemical exchanges. Combined, they can greatly refine the characterization of these exchanges. Here we report profiles of ε_{Nd} at 21 stations located in the Coral and Solomon Seas as part of the GEOTRACES GP-12 cruise that complement the rare earth element concentration (REE) profiles of Pham (Chemical Geology, 2019, 524 (May), 11–36). Waters exiting the Solomon Sea are generally slightly more radiogenic than the incoming ones, suggesting inputs of radiogenic material along their pathways across the Solomon Sea. This radiogenic material is brought to the surface waters via natural processes (rivers, volcanic dusts) and likely local mining activities. Noticeable ε_{Nd} increases are also observed in subsurface and intermediate layers. All these processes indicate the occurrence of local Boundary Exchange (BE) processes, which are estimated to occur within a few days. Coupling hydrological and chemical tracers allows highlighting the land-ocean interactions affecting some water layers and quantifying the exchanged fluxes of Nd. Modifications of the Nd concentration and isotopic composition in the lower thermocline layer require an external flux of 7.9 ± 2.0 t(Nd)/yr only partly balanced by a scavenging flux of 1.8 ± 2.3 t(Nd)/yr, leading to a net influx of 6.1 ± 1.7 t(Nd)/yr. Regarding the Upper Circumpolar Deep Water, a total net flux of 105 ± 50 t(Nd)/yr is estimated, the external flux is relatively high (86 ± 31 t(Nd)/yr while the scavenging flux remains. These results refine the role of the Solomon Sea as a supplier of continental chemical elements to the Pacific equatorial waters.

Keywords: neodymium isotopic composition, rare earth elements, Solomon Sea, GEOTRACES, boundary exchange quantification

1 INTRODUCTION

The Equatorial Pacific is an important oceanic area for the atmosphere-ocean carbon dioxide (CO_2) exchange. In its eastern part, upwelling and degassing of CO_2-rich cold deep waters act as a CO_2 source to the atmosphere (Takahashi et al., 1993; Radenac et al., 2012). Besides, while the equatorial surface waters are rich in macronutrients (as NO_3^- or PO_4^{3}), the chlorophyll level stay low up to the Galapagos islands (Radenac et al., 2012). Thus, most of the western and central equatorial Pacific is considered as a "High Nutrient Low Chlorophyll" area. This low productivity is explained by the fact that the surface waters are depleted in elements essential for the phytoplankton growth -such as Fe, Ni, Cu, Co, Cd, Zn, also called micronutrients (Pitchford and Brindley, 1999; Ryan et al., 2006; Boyd et al., 2007; Venables and Moore, 2010). These essential elements are lithogenic, i.e., they have a terrestrial source.

Nutrient depletion in the equatorial Pacific surface waters is attributed to the remote locations of their sources. By contrast, the Equatorial UnderCurrent (EUC), a current vein confined in the equatorial band is enriched in macro- and micronutrients (Slemons et al., 2010). The EUC starts at about 200 m depth in the west (at 156°E; Grenier et al., 2011) and progressively upwells while flowing eastwards, to eventually reach the surface in the eastern equatorial "cold tongue" and fertilize the area (Tsuchiya et al., 1989). This dynamic is the main cause of the west-east gradient of productivity. In its western part, the EUC is mostly fed by waters originating from the low-latitude western boundary currents, in majority from the southern hemisphere, from waters flowing along the North Australian and Papua New Guinea coasts (Grenier, 2012; Grenier et al., 2013; Grenier et al., 2014). Because of the high weathering rates and the occurrence of strong boundary currents flowing along these coasts (Milliman, 1995; Cravatte et al., 2011), it is strongly suspected that sediments freshly deposited along the coasts and margins of the southwest Pacific lands are a source of lithogenic elements to the EUC (e.g., Johnson et al., 1999; Lacan and Jeandel, 2001; Filippova et al., 2017; Behrens et al., 2020).

The use of rare earth element concentrations (REE) and neodymium isotopic compositions (Nd-IC) in marine geochemistry has been conducted for more than 30 years (Jeandel, 1993; Sholkovitz et al., 1999; Elderfield et al., 2006; Stichel et al., 2012; Stichel et al., 2015; Fröllje et al., 2016; Behrens et al., 2018a; Behrens et al., 2018b; Lambelet et al., 2018; Amakawa et al., 2019; Pham et al., 2019; Stichel et al., 2020; Rahlf et al., 2021). The isotopic composition of Nd is a very powerful tracer that allows the characterization of the sources of lithogenic elements to the ocean. One of the seven Nd isotopes, ^{143}Nd, is formed by α-decay of ^{147}Sm. The Sm abundance in rocks is strongly linked to their nature and chemical composition. Consequently, its natural abundance varies and depends on the time-integrated Sm/Nd ratio of the rock from which the Nd is derived. This variation is expressed as ε_{Nd}:

$$\varepsilon_{Nd} = \left(\frac{(^{143}\mathrm{Nd}/^{144}\mathrm{Nd})_{\mathrm{sample}}}{(^{143}\mathrm{Nd}/^{144}\mathrm{Nd})_{\mathrm{CHUR}}} - 1 \right) \times 10^4$$

where CHUR stands for chondritic uniform reservoir and represents the modelized average earth value, presently 0.512630 ± 11 ($2\sigma_m$,Bouvier et al., 2008).

Several current veins come together to form the EUC. This current is enriched in macro- and micronutrients, properties acquired while flowing along the Southwest Pacific coasts. Boundary Exchange (BE) is suspected to be the enrichment mechanism (Lacan and Jeandel, 2001; Lacan and Jeandel, 2005; Grenier et al., 2013; Behrens et al., 2020). This term was used to state that when a water flows along a margin, its Nd isotopic signature could be modified by Nd inputs released from the benthic sediments even if its Nd concentration does not (or barely) change. This means that Nd release is followed by Nd scavenging, at a time scale that still needs to be determined. One of the basic conditions to observe BE is that, upstream the contact with the margin sediment, the water mass has a different Nd-IC from the Nd-IC of the margin sediment (Arsouze et al., 2007). If both Nd-IC are the same, it does not preclude BE to occur but it is not observable with Nd parameters. However, this definition results from observations and does not designate a specific process as underlined by Lacan and Jeandel, (2005). Instead, Jeandel, (2016) suggests that BE comprises the mechanisms allowing land-to-ocean inputs of elements along the oceanic margins (e.g. reductive or non-reductive sediment dissolution, diagenetic pore water fluxes, processes inside intermediate or benthic nepheloid layer; Homoky et al., 2013; Labatut et al., 2014; Homoky et al., 2016) competing the mechanisms that would subtract elements from the seawater (e.g., *via* boundary scavenging processes which themselves comprise adsorption or precipitation on resuspended reactive particles or during diagenetic processes). In addition, Abbott (2019) suggested that BE processes are occurring not only along the margins but also in the sediments that line the bottom of the abyss. Boundary Exchange resulting net fluxes should be positive when Nd release from the sediment is greater than Nd removal by scavenging, and negative in the opposite case. The exchanged flux cannot be quantified with the concentration only, it requires the complementary information brought by the isotopes (Jeandel, 2016; Jeandel and Vance, 2018).

Located at the western South Pacific boundary between 10°S and 5°S, the Solomon Sea connects the tropical and equatorial regions (**Figure 1**). It is a semi-enclosed sea characterized by a complicated bathymetry and a complex circulation, with the convergence of several water masses within strong boundary currents (Lindstrom et al., 1987; Germineaud et al., 2016). Therefore, waters flowing through the Solomon Sea are subject to many potential chemical inputs. Volcanic islands in this region are young and subject to extreme weather conditions favourable to generate substantial lithogenic weathering and transport of weathered products via diffuse surface run-off and rivers such as the Sepik and Fly (Milliman et al., 1999; Sholkovitz et al., 1999). Another possible source of lithogenic material could be attributed to extractive activities: dust originating from mining heap and muddy mine wastes could represent a significant source of terrigenous sediment to the Solomon Sea. **Figure 4A** displays location of some large mines in islands surrounding the Solomon Sea. Most of these mines are in operation, as for example Lihir

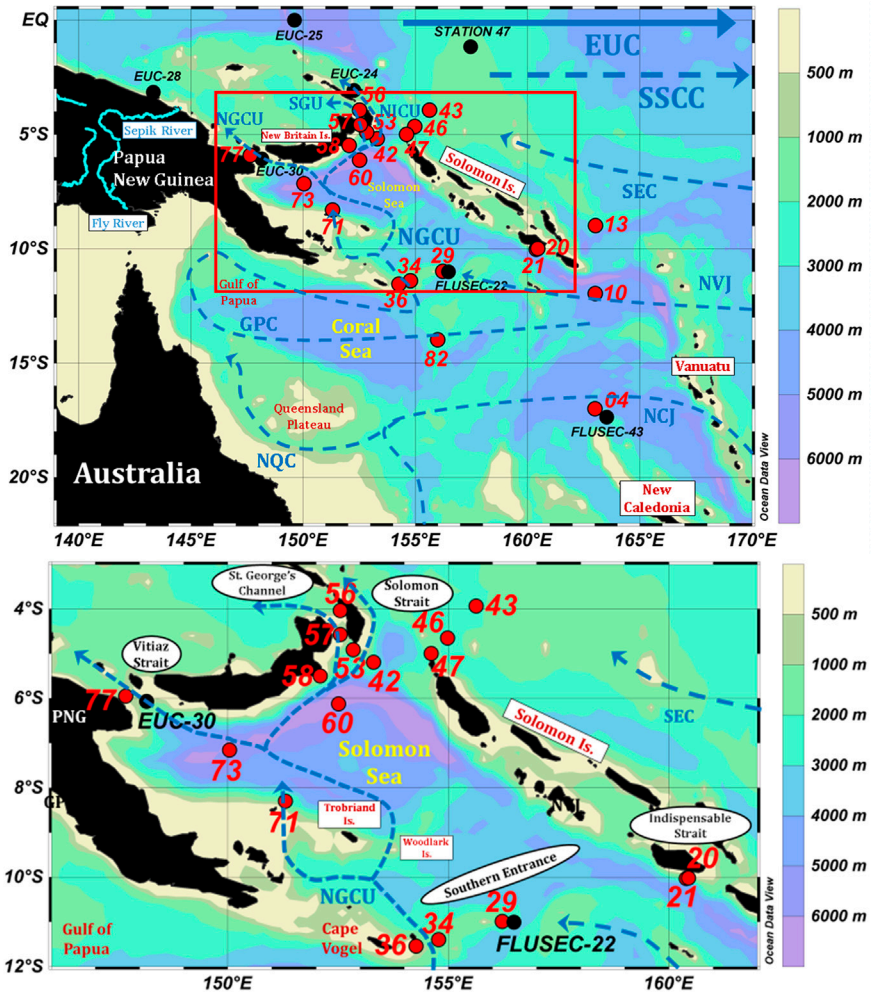

FIGURE 1 | Sample location map. The bottom panel zooms in the Solomon Sea, correspond to the red rectangle in the upper panel. PANDORA sampling locations are highlighted by red dots and numbers. Samples analyzed in previous works are reported, highlighted by black circles and station annotation. Those samples belong to five stations corresponding to EUC-Fe and FLUSEC-01 cruises (EUC-24, EUC-25, EUC-28, FLUSEC-22 and FLUSEC-43), studied by Grenier et al. (2013) and one station (Station 47) corresponding to CASSIOPEE cruise, studied by Behrens et al. (unpublished). Dashed arrows represent the main currents flowing in the Southwest Pacific Ocean (Grenier et al., 2011, 2013). EUC, Equatorial Undercurrent; SSCC, South Subsurface Countercurrent; SEC, South Equatorial Current; NVJ, North Vanuatu Jet; NCJ, North Caledonian Jet; NQC, North Queensland Current; GPC, Gulf of Papua Current; NGCU, New Guinea Coastal Undercurrent; NICU, New Ireland Coastal Undercurrent; SGU, St. George's Undercurrent.

mine in Lihir Island (https://www.mining-technology.com/projects/lihir-gold-mine/), Kolosori mine in Isabel Island (https://miningdataonline.com/property/1420/Kolosori-Project.aspx) or Edie Creek in Papua New Guinea (https://www.niuminco.com.au/current-operations.html). Other mines have been closed due to their environmental and societal impacts, e.g.: the Gold Ridge Mine. However, the latter (and others) will likely be exploited again soon due to their resource potential (https://www.abc.net.au/news/2019-10-30/china-cites-early-harvest-benefits-in-guadalcanal-deal/11654596).

Pham et al. (2019) described and quantified the modification of dissolved REE during the transit of water through the Solomon Sea. These authors identified the basaltic footprint in the dissolved REE enrichment observed in the surface waters. They also revealed a significant Nd enrichment in the lower thermocline layer that further feeds the EUC. However, since the Nd isotopic compositions were not available at the time of this first study, Pham et al. (2019) could not work more closely on the dissolved-particle exchange processes. The present study combines new Nd isotopic composition (Nd-IC, ε_{Nd}) data with the published dissolved Nd concentrations (Pham et al., 2019) in order to: i) describe the modification of the Nd parameters of the water masses composing the different currents during their transit through the Solomon Sea to the Equator; ii) highlight the origin of the supplied materials; iii) when possible, quantify the land-ocean fluxes inferred from the Nd concentration and ε_{Nd} changes.

TABLE 1 | Location, depth, hydrological properties, Eu anomaly, Nd concentration, Nd-IC ($^{143}Nd/^{144}Nd$) and ε_{Nd} of the samples analyzed in this study (Pham et al., 2019).

No.	Depth (m)	Salinity (PSU)	Pot.temp (θ) (°C)	Pot. dens σ_θ (kg/m^3)	Eu/Eu* ± 2σ	[Nd] ± 2σ (pmol/kg)	ε_{Nd} ± 2σ	Layer
Station 004 (July 01, 2012; 17° 0′ 10.8 S; 162° 59′ 45.6″ E; depth: 4,680 m)								
1	30	34.8	25.9	22.9	1.21 ± 0.07	3.8 ± 0.1	1.0 ± 0.2	SL
2	166	35.6	21.5	24.8	1.12 ± 0.05	3.2 ± 0.1	–1.0 ± 0.3	UTL
3	250	35.5	17.8	25.7	1.11 ± 0.05	3.4 ± 0.1	–2.1 ± 0.3	LTL-1
4	351	35.1	13.9	26.3″	1.09 ± 0.04	4.5 ± 0.1	–2.8 ± 0.3	LTL-2
5	621	34.4	6.50	27.0	1.00 ± 0.05	7.3 ± 0.2	–6.2 ± 0.2	IL
6	730	34.4	5.37	27.2	1.11 ± 0.08	7.7 ± 0.4	–5.6 ± 0.2	IL
7	1,134	34.5	3.57	27.4	1.05 ± 0.06	10 ± 0.3	–4.0 ± 0.2	IL
8	1,734	34.6	2.41	27.6	—	—	–5.0 ± 0.3	DL
9	3,598	34.7	1.55	27.8	1.12 ± 0.06	24 ± 0.7	—	BL
Station 010 (July 03, 2012; 12° 0′ 0″ S; 162° 59′ 56.4″ E; depth: 5,092 m)								
10	35	34.6	28.1	22.1	1.21 ± 0.07	3.6 ± 0.1	0.9 ± 0.2	SL
11	185	36.0	24.5	24.5	—	—	–1.3 ± 0.3	UTL
12	260	35.5	18.4	25.6	1.21 ± 0.07	3.6 ± 0.1	–2.7 ± 0.4	LTL-1
13	350	34.9	12.7	26.4	1.05 ± 0.06	4.9 ± 0.2	–4.5 ± 0.2	LTL-2
14	515	34.5	7.40	27.0	—	—	–5.4 ± 0.2	IL
15	680	34.5	5.40	27.2	0.95 ± 0.06	7.7 ± 0.2	–5.1 ± 0.2	IL
16	1,000	34.5	3.96	27.4	—	—	–4.5 ± 0.2	IL
17	1,735	34.6	2.44	27.6	1.12 ± 0.06	13 ± 0.3	–3.5 ± 0.2	DL
18	2,500	34.7	1.78	27.7	1.13 ± 0.07	18 ± 0.6	–4.0 ± 0.2	BL
19	4,000	34.7	1.44	27.8	1.08 ± 0.06	24 ± 0.7	–4.8 ± 0.2	BL
Station 013 (July 04, 2012; 9° 0′ 10.8″ S; 162° 59′ 56.4″ E; depth: 3,853 m)								
20	5	34.7	29.2	21.7	1.14 ± 0.06	3.9 ± 0.1	–1.8 ± 0.4	SL
21	40	34.7	29.2	21.8	1.05 ± 0.06	3.3 ± 0	–0.8 ± 0.6	SL
22	160	35.8	24.1	24.2	1.26 ± 0.07	2.8 ± 0.1	–1.6 ± 0.4	UTL
23	300	35.2	15.2	26.1	0.96 ± 0.04	3.7 ± 0.1	–3.1 ± 0.4	LTL-1
24	600	34.5	6.13	27.2	1.08 ± 0.03	7.2 ± 0.1	–4.3 ± 0.2	IL
25	685	34.5	5.53	27.2	1.18 ± 0.06	7.2 ± 0.2	–4.2 ± 0.3	IL
26	1,335	34.6	3.11	27.5	1.02 ± 0.04	9.6 ± 0.2	–3.9 ± 0.2	DL
27	1,535	34.6	2.71	27.6	1.11 ± 0.05	10 ± 0.3	–4.3 ± 0.2	DL
28	2,000	34.6	2.02	27.7	1.21 ± 0.06	14 ± 0.4	–2.7 ± 0.2	BL
Station 020 (July 06, 2012; 9° 59′ 56.4″ S; 160° 25′ 1.2″ E; depth: 2,910 m)								
29	25	34.8	28.9	22.0	1.21 ± 0.06	4.7 ± 0.2	1.7 ± 0.3	SL
30	190	35.8	22.6	24.7	—	—	–1.5 ± 0.4	UTL
31	600	34.5	6.22	27.1	1.02 ± 0.06	7.2 ± 0.2	–4.8 ± 0.2	IL
32	900	34.5	4.79	27.3	1.08 ± 0.07	8.2 ± 0.3	–4.6 ± 0.2	IL
33	1,600	34.6	2.72	27.6	—	8.2 ± 0.3	–3.9 ± 0.2	DL
Station 021 (July 07, 2012; 10° 0′ 46.8″ S; 160° 21′ 25.2″ E; depth: 3,342 m)								
34	250	35.4	17.2	25.8	1.08 ± 0.05	4.1 ± 0.1	–2.3 ± 0.4	LTL-1
35	400	34.7	9.04	26.9	1.07 ± 0.05	5.3 ± 0.1	–4.3 ± 0.2	LTL-2
36	550	34.5	6.38	27.1	1.06 ± 0.03	6.8 ± 0.1	–4.9 ± 0.3	IL
37	2,115	34.6	2.07	27.7	1.18 ± 0.04	15 ± 0.7	–4.4 ± 0.2	BL
38	2,625	34.7	1.79	27.7	1.21 ± 0.10	18 ± 0.9	–4.4 ± 0.2	BL
39	3,280	34.7	1.61	27.8	1.14 ± 0.10	19 ± 0.7	–6.0 ± 0.3	BL
Station 029 (July 09, 2012; 11° 3′ 39.6″ S; 156° 12′ 54″ E; depth: 3,856 m)								
40	267	35.4	17.1	25.8	1.10 ± 0.05	4.0 ± 0.1	–4.1 ± 0.3	LTL-1
41	737	34.5	5.35	27.2	1.07 ± 0.05	7.2 ± 0.2	–5.3 ± 0.3	IL
42	934	34.5	4.28	27.4	1.08 ± 0.06	8.6 ± 0.2	–5.3 ± 0.2	IL
43	1,140	34.5	3.70	27.5	1.16 ± 0.05	9.2 ± 0.2	–4.0 ± 0.2	IL
44	1,534	34.6	2.82	27.6	1.16 ± 0.06	11 ± 0.3	–3.7 ± 0.2	DL
45	2,999	34.7	1.69	27.8	1.14 ± 0.08	17 ± 0.9	–5.5 ± 0.2	BL
Station 034 (July 10, 2012; 11° 27′ 7.2″ S; 154° 39′ 54″ E; depth: 2,005 m)								
46	40	34.9	28.5	22.2	1.21 ± 0.04	4.2 ± 0.1	0.7 ± 0.2	SL
47	180	35.7	21.8	24.8	1.21 ± 0.03	3.4 ± 0	–1.2 ± 0.5	UTL
48	300	35.2	15.4	26.1	1.14 ± 0.05	4.5 ± 0.1	–3.0 ± 0.2	LTL-1
49	635	34.5	7.12	27.0	1.01 ± 0.04	7.2 ± 0.1	–5.8 ± 0.2	IL
50	735	34.4	5.65	27.2	1.04 ± 0.04	8.6 ± 0.2	–7.1 ± 0.2	IL
51	1,065	34.5	4.14	27.4	1.05 ± 0.04	9.3 ± 0.2	–4.6 ± 0.2	IL
52	1,550	34.6	2.73	27.6	1.05 ± 0.06	13 ± 0.5	–3.2 ± 0.2	DL
53	1,665	34.6	2.56	27.6	1.11 ± 0.05	14 ± 0.3	–3.7 ± 0.2	DL
54	1,750	34.6	2.38	27.6	1.11 ± 0.04	15 ± 0.4	–3.4 ± 0.2	DL
55	1,920	34.6	2.14	27.7	—	15 ± 0.4	–3.7 ± 0.3	BL

(Continued on following page)

TABLE 1 | (*Continued*) Location, depth, hydrological properties, Eu anomaly, Nd concentration, Nd-IC ($^{143}Nd/^{144}Nd$) and ε_{Nd} of the samples analyzed in this study (Pham et al., 2019).

No.	Depth (m)	Salinity (PSU)	Pot.temp (θ) (°C)	Pot. dens σ_θ (kg/m^3)	Eu/Eu* ± 2σ	[Nd] ± 2σ (pmol/kg)	ε_{Nd} ± 2σ	Layer
Station 036 (July 11, 2012; 11° 30′ 7.2″ S; 154° 23′ 24″ E; depth: 1,168 m)								
56	25	34.5	27.8	22.1	1.25 ± 0.04	8.2 ± 0.1	1.1 ± 0.3	SL
57	100	35.4	24.3	23.9	1.18 ± 0.04	3.9 ± 0.1	–0.6 ± 1.6	UTL
58	160	35.6	22.3	24.6	1.22 ± 0.04	3.8 ± 0.1	–1.2 ± 0.3	UTL
59	180	35.6	21.1	25.0	1.11 ± 0.04	3.8 ± 0.1	–1.2 ± 0.3	UTL
60	400	34.9	12.2	26.5	1.08 ± 0.04	5.2 ± 0.1	–5.0 ± 0.2	LTL-2
61	700	34.5	6.29	27.1	0.98 ± 0.03	7.2 ± 0.1	–4.5 ± 0.2	IL
62	900	34.5	5.13	27.2	1.07 ± 0.04	7.5 ± 0.1	–4.8 ± 0.2	IL
Station 042 (July 15, 2012; 5° 8′ 42″ S; 153° 17′ 24″ E; depth: 3,081 m)								
63	5	34.7	29.4	21.7	1.26 ± 0.09	3.9 ± 0.2	0.6 ± 0.3	SL
64	180	35.6	22.0	24.7	1.21 ± 0.06	3.4 ± 0.1	–1.9 ± 0.3	UTL
65	225	35.4	16.8	25.8	0.79 ± 0.04	3.8 ± 0.1	–2.1 ± 0.5	LTL-1
66	400	34.6	9.02	26.8	0.98 ± 0.04	6.1 ± 0.1	–1.9 ± 0.3	LTL-2
67	500	34.5	7.27	27.0	1.03 ± 0.04	6.8 ± 0.1	–5.3 ± 0.2	IL
68	750	34.5	5.32	27.2	1.06 ± 0.03	7.3 ± 0.1	–4.5 ± 0.2	IL
69	1,000	34.5	4.03	27.4	1.07 ± 0.08	9.4 ± 0.3	–3.2 ± 0.2	IL
70	1,200	34.6	3.50	27.5	1.22 ± 0.06	10 ± 0.2	–2.0 ± 0.2	DL
71	1,550	34.6	2.61	27.6	1.22 ± 0.05	14 ± 0.3	–2.3 ± 0.2	DL
72	1,750	34.6	2.42	27.6	1.16 ± 0.05	15 ± 0.5	–2.4 ± 0.2	DL
73	2,000	34.6	2.13	27.7	1.22 ± 0.07	18 ± 0.8	–2.1 ± 0.2	BL
74	2,500	34.7	1.78	27.7	1.20 ± 0.08	21 ± 0.9	–2.7 ± 0.2	BL
Station 043 (July 17, 2012; 3° 59′ 52.8″ S; 155° 35′ 38.4″ E; depth: 1,925 m)								
75	5	34.7	29.3	21.7	1.13 ± 0.07	3.5 ± 0.1	–0.1 ± 0.5	SL
76	150	35.9	25.1	24.0	1.11 ± 0.05	3.8 ± 0.2	–2.5 ± 0.2	UTL
77	230	35.2	14.8	26.1	1.19 ± 0.06	5.2 ± 0.1	–4.6 ± 0.2	LTL-1
78	700	34.5	5.91	27.2	1.24 ± 0.04	7.6 ± 0.1	–3.2 ± 0.2	IL
79	1,200	34.6	3.74	27.5	1.15 ± 0.04	9.6 ± 0.2	–2.5 ± 0.2	DL
Station 046 (July 18, 2012; 4° 42′ 0″ S; 154° 52′ 48″ E; depth: 3,117 m)								
80	50	34.8	29.2	21.8	1.19 ± 0.04	3.3 ± 0.1	–0.5 ± 0.3	SL
81	150	36.0	25.4	24.0	1.11 ± 0.03	2.6 ± 0.1	–0.5 ± 0.4	UTL
82	400	34.6	8.72	26.9	1.11 ± 0.04	6.5 ± 0.1	–3.0 ± 0.2	IL
83	700	34.5	6.03	27.2	1.10 ± 0.05	7.2 ± 0.2	–2.3 ± 0.4	IL
84	1,000	34.5	4.33	27.4	1.07 ± 0.04	8.9 ± 0.2	–2.7 ± 0.2	IL
Station 047 (July 18, 2012; 4° 56′ 2.4″ S; 154° 38′ 52.8″ E; depth: 1,004 m)								
85	25	34.7	29.1	21.8	1.27 ± 0.04	4.4 ± 0.1	1.3 ± 0.3	SL
86	156	36.0	24.0	24.4	0.99 ± 0.02	3.0 ± 0.1	–1.6 ± 0.6	UTL
87	264	35.1	14.0	26.3	1.05 ± 0.03	4.8 ± 0.1	–3.1 ± 0.2	LTL-1
88	635	34.5	5.86	27.2	1.09 ± 0.04	7.7 ± 0.1	–3.3 ± 0.2	IL
Station 053 (July 19, 2012; 4° 54′ 18″ S; 152° 52′ 12″ E; depth: 733 m)								
89	25	34.9	29.0	22.0	1.27 ± 0.08	5.7 ± 0.3	2.8 ± 0.2	SL
90	149	35.6	21.9	24.7	1.12 ± 0.05	4.0 ± 0.1	–0.8 ± 0.2	UTL
91	335	35.0	12.6	26.5	1.10 ± 0.03	5.3 ± 0.1	–4.0 ± 0.2	LTL-2
92	719	34.5	5.42	27.2	1.07 ± 0.03	7.8 ± 0.1	–4.0 ± 0.2	IL
Station 056 (July 20, 2012; 4° 4′ 37.2″ S; 152° 32′ 20.4″ E; depth: 1,580 m)								
93	1,582	34.6	2.82	27.6	1.08 ± 0.04	14 ± 0.3	–1.9 ± 0.2	DL
Station 057 (July 20, 2012; 4° 34′ 12″ S; 152° 31′ 22.8″ E; depth: 2,552 m)								
94	25	34.8	29.0	21.9	1.39 ± 0.08	5.2 ± 0.1	1.1 ± 0.2	SL
95	150	35.6	23.6	24.2	1.19 ± 0.08	3.7 ± 0.1	–4.4 ± 0.2	UTL
96	250	35.3	15.8	26.0	1.09 ± 0.1	4.2 ± 0.1	0.5 ± 0.3	LTL-1
97	450	34.7	8.97	26.9	1.02 ± 0.04	6.2 ± 0.1	–4.6 ± 0.2	IL
98	580	34.5	7.08	27.0	1.06 ± 0.04	6.8 ± 0.1	–5.4 ± 0.2	IL
99	850	34.5	4.62	27.3	1.15 ± 0.05	8.1 ± 0.2	–4.5 ± 0.3	IL
100	1,302	34.6	3.37	27.5	1.18 ± 0.05	11 ± 0.3	–2.5 ± 0.2	DL
101	1,650	34.6	2.61	27.6	—	—	–2.4 ± 0.2	DL
102	2,201	34.7	1.99	27.7	1.20 ± 0.05	20 ± 0.5	–1.5 ± 0.2	BL
Station 058 (July 21, 2012; 5° 30′ 10.8″ S; 152° 5′ 52.8″ E; depth: 1,142m)								
103	215	35.5	18.6	25.5	1.16 ± 0.06	3.9 ± 0.1	–4.0 ± 0.3	LTL-1
104	1,100	34.5	3.67	27.5	1.07 ± 0.05	11 ± 0.3	–2.3 ± 0.2	DL
Station 060 (July 22, 2012; 6° 10′ 1.2″ S; 152° 29′ 49.2″ E; depth: 5,609 m)								
105	35	34.7	28.0	22.2	1.26 ± 0.06	4.6 ± 0.2	1.2 ± 0.3	SL
106	180	35.7	22.3	24.7	1.18 ± 0.09	3.4 ± 0.1	–1.7 ± 0.3	UTL
107	250	35.3	16.6	25.9	1.28 ± 0.06	5.1 ± 0.1	–2.2 ± 0.2	LTL-1

(Continued on following page)

TABLE 1 | (*Continued*) Location, depth, hydrological properties, Eu anomaly, Nd concentration, Nd-IC ($^{143}Nd/^{144}Nd$) and ε_{Nd} of the samples analyzed in this study (Pham et al., 2019).

No.	Depth (m)	Salinity (PSU)	Pot.temp (θ) (°C)	Pot. dens σ_θ (kg/m^3)	Eu/Eu* ± 2σ	[Nd] ± 2σ (pmol/kg)	ε_{Nd} ± 2σ	Layer
108	480	34.5	7.19	27.0	1.04 ± 0.04	6.5 ± 0.2	−4.8 ± 0.2	IL
109	1,000	34.5	3.93	27.4	1.20 ± 0.04	9.4 ± 0.1	−3.2 ± 0.2	IL
110	1,600	34.6	2.60	27.6	1.30 ± 0.05	14 ± 0.5	−1.9 ± 0.4	DL
111	1,800	34.6	2.26	27.7	1.20 ± 0.03	16 ± 0.7	−1.8 ± 0.2	BL
112	2,541	34.7	1.72	27.7	1.23 ± 0.04	24 ± 0.8	−1.9 ± 0.2	BL
113	3,250	34.7	1.67	27.8	1.29 ± 0.06	27 ± 1.1	−0.9 ± 0.2	BL
114	4,000	34.7	1.67	27.8	1.28 ± 0.06	28 ± 0.8	−0.7 ± 0.2	BL
115	4,500	34.7	1.66	27.8	1.26 ± 0.08	30 ± 0.9	−0.9 ± 0.2	BL
116	4,750	34.7	1.66	27.8	1.29 ± 0.04	30 ± 0.4	−1.0 ± 0.2	BL
117	5,000	34.7	1.65	27.8	1.29 ± 0.04	25 ± 0.3	−1.5 ± 0.2	BL
118	5,603	34.7	1.65	27.8	1.19 ± 0.06	26± 0.7	−2.2 ± 0.2	BL
Station 071 (July 25, 2012; 8° 19′ 55.2″ S; 151° 17′ 27.6″ E; depth: 1,563 m)								
119	50	34.8	27.6	22.4	1.26 ± 0.10	4.0 ± 0.2	0.6 ± 0.5	SL
120	160	35.7	22.4	24.6	1.09 ± 0.10	3.9 ± 0.2	0.1 ± 1.5	UTL
121	400	35.0	12.6	26.5	1.08 ± 0.08	5.2 ± 0.2	−3.5 ± 0.2	LTL-2
122	600	34.5	6.70	27.1	1.00 ± 0.08	6.9 ± 0.4	−5.5 ± 0.2	IL
123	1,100	34.5	4.05	27.4	1.17 ± 0.05	9.7 ± 0.2	−3.2 ± 0.2	IL
Station 073 (July 26, 2012; 7° 9′ 57.6″ S; 149° 59′ 56.4″ E; depth: 5,253 m)								
124	50	35.1	27.3	22.7	1.22 ± 0.05	4.1 ± 0.1	0.2 ± 0.5	SL
125	170	35.6	21.7	24.8	1.33 ± 0.18	8.6 ± 0.9	−1.3 ± 0.3	UTL
126	200	35.6	21.2	24.9	1.15 ± 0.05	3.3 ± 0.1	−1.4 ± 0.3	UTL
127	700	34.5	5.88	27.2	1.01 ± 0.05	13 ± 0.4	−4.8 ± 0.2	IL
128	1,650[1]	34.6	2.60	27.6	1.15 ± 0.07	28 ± 1.2	−2.0 ± 0.2	DL
129	1,650*[,2]	34.6	2.60	27.6	—	—	−1.6 ± 0.2	DL
Station 077 (July 28, 2012; 5° 57′ 3.6″ S; 147° 39′ 36″ E; depth: 1,045 m)								
130	25	34.8	27.6	22.3	1.24 ± 0.04	4.9 ± 0.1	1.5 ± 0.3	SL
131	25*	34.8	27.6	22.3	—	5.0 ± 0.1	0.2 ± 0.3	SL
132	180	35.6	21.4	24.9	1.12 ± 0.03	3.4 ± 0.1	−1.5 ± 0.4	UTL
133	180*	35.6	21.4	24.9	—	5.3 ± 0.1	−0.7 ± 0.4	UTL
134	501	34.6	8.02	26.9	1.09 ± 0.03	8.0 ± 0.1	−5.3 ± 0.3	LTL-2
135	501*	34.6	8.02	26.9	—	7.8 ± 0.1	−4.9 ± 0.2	LTL-2
136	701	34.5	5.54	27.2	1.05 ± 0.03	7.9 ± 0.1	−4.6 ± 0.2	IL
137	701*	34.5	5.54	27.2	—	8.9 ± 0.1	−4.0 ± 0.3	IL
138	983	34.5	4.47	27.3	1.13 ± 0.05	9.6 ± 0.2	−3.0 ± 0.2	IL
139	983*	34.5	4.47	27.3	—	11.5 ± 0.3	−3.1 ± 0.2	IL
Station 082 (August 03, 2012; 13° 59′ 49.2″ S; 156° 0′ 25.2″ E; depth: 2,586 m)								
140	25*	34.9	26.2	22.90	1.40 ± 0.04	4.2 ± 0.1	−0.1 ± 0.2	SL
141	180*	35.8	22.6	24.60	1.04 ± 0.03	3.5 ± 0.1	−1.7 ± 0.2	UTL
142	700*	34.5	6.03	27.10	1.00 ± 0.03	8.1 ± 0.2	−5.2 ± 0.2	IL
143	800*	34.5	5.08	27.20	1.02 ± 0.04	8.6 ± 0.3	−5.3 ± 0.1	IL
144	1,000*	34.5	4.11	27.40	1.04 ± 0.04	9.5 ± 0.2	5.0 ± 0.2	IL
145	1,200*[,3]	34.5	3.45	27.50	1.05 ± 0.02	10 ± 0.2	−4.6 ± 0.2	DL
146	1,350*	34.6	3.16	27.50	0.98 ± 0.03	11 ± 0.4	−3.9 ± 0.1	DL
147	2,000*	34.6	2.23	27.70	1.18 ± 0.04	14 ± 0.4	—	BL

All the errors are reported within 2 sigmas.

*, *Unfiltered samples;* [1]*: n = 6;* [2]*: n = 2;* [3]*: n = 3.*

2 METHODOLOGY

2.1 Materials and Methods

The PANDORA cruise (GEOTRACES cruise GP12, Ganachaud et al., 2017) took place within the Solomon Sea from June 26th to August 07th, 2012 onboard the R/V L'Atalante (https://www.bodc.ac.uk/geotraces/cruises/programme/). The cruise followed a latitudinal transect along 163°E between 18°S and 9°S to document the westward South Equatorial Current (SEC) branches entering into the Coral Sea, including the North Caledonian and North Vanuatu Jets, NCJ and NVJ, respectively (Kessler and Cravatte, 2013a). After crossing the Indispensable Strait, the cruise surveyed the whole "Southern Entrance" of the Solomon Sea, joined the western area of the Gulf of Papua New Guinea (PNG) between 155° and 161°S along ~11°S, crossed the Solomon Sea again to document its central part and eventually explored the three exits: Vitiaz Strait, St. George's Channel and Solomon Strait (**Figure 1**, Ganachaud et al., 2017).

Samples for Nd-IC and [REE] were collected at 21 stations (twenty filtered and one unfiltered) (**Table 1**; Ganachaud et al., 2017). The unfiltered samples from station 82 were used for reproducibility tests only. Samples were collected in the core of the water masses encountered at each station using 12 L-Niskin bottles mounted on a CTD/rosette system. As

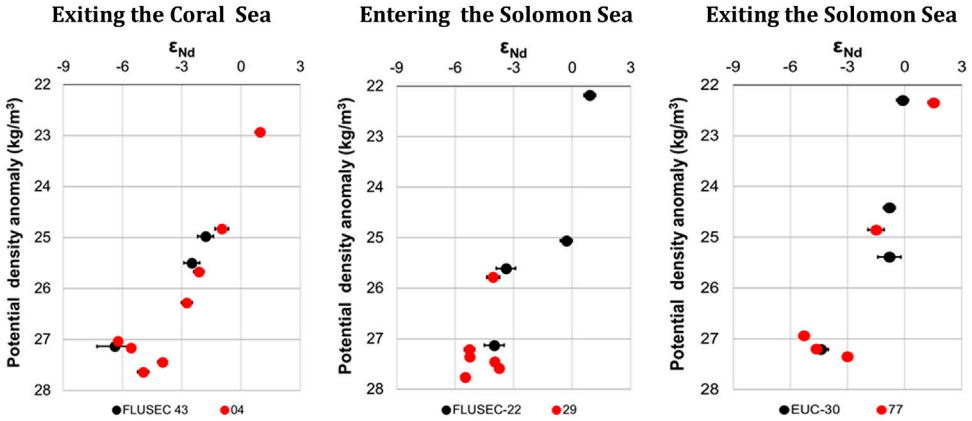

FIGURE 2 | Comparison of the ε_{Nd} values of samples collected during the Pandora cruise (red dots) with those reported in Grenier et al. (2013; black dots).

soon as collected, the samples were filtered through 0.45 µm pore size, 47 mm diameter SUPOR® membranes. An aliquot of 0.5 L was transferred into pre-cleaned low-density polyethylene (LDPE) bottles and preserved for dissolved REE analyses, data published in (Pham et al., 2019) and are freely accessible. (https://www.bodc.ac.uk/geotraces/). The remaining volume (11 L) was dedicated to the Nd isotope extraction.

2.2 Neodymium Isotopic Composition Analytical Procedure

On board, the pH of each sample dedicated to the Nd-IC determination was raised to 3.4–3.7 with the addition of a small volume of suprapur NH_4OH (Merck®) prior to be passed through the preconcentration system, made of two pre-cleaned C18 cartridges packed with 300 mg of the complexing mixture of 65% bi (2-ethylhexyl) hydrogen phosphate (HDEHP) and 35% 2-ethylhexyl dihydrogen phosphate (H_2MEHP; Shabani et al., 1992; Tachikawa et al., 1999). Samples were pumped through the cartridge at a flow rate of 20 ml/min using a peristaltic pump. The Nd present in the sample was quantitatively adsorbed by the complexing agent while major ions and a large amount of the barium present in seawater were drained (Shabani et al., 1992; Tachikawa et al., 1999). Cartridges were then disconnected from the circuit, sealed with Parafilm®, and stored in a clean plastic bag.

Back to the land-based laboratory, REEs include Nd were eluted from the C18 cartridges. Approximately 5 ml of 0.01 M HCl was first passed through the cartridge at 5 ml/min to remove the remaining major salts including barium. Then, 20 ml of 6 M HCl was passed at the same flow rate to elute the REEs (and/or remaining traces of other elements) into a PTFE vial (Jeandel et al., 1998). The eluted solution was evaporated to almost dryness and 2 ml of aqua regia was added to remove any organic matter. The resulting solution was placed on a hot plate at 120°C overnight and evaporated to dryness. Subsequently, two chemical extractions were performed to purify Nd from other REEs: 1) a chromatographic extraction using a cationic column containing 1.5 ml of Dowex AG50W-X8 resin (200–400 mesh), to separate the REEs from the remaining matrix (Tachikawa et al., 1999), and 2) a separation of Nd from other REEs using a quartz column packed with 400 mg of Ln-spec resin (140–270 mesh; Pin and Santos Zalduegui, 1997). The eluted solution was then evaporated gradually to a small drop of 1–2 µl for the mass spectrometry measurement.

The isotopic compositions of Nd were measured on the Thermo-Ionization Mass Spectrometer (TIMS, Thermo Fisher®) of the Midi-Pyrénées Observatory (OMP) in Toulouse. Sample was cautiously deposited onto a rhenium filament. Once in the TIMS, the Nd isotopes were evaporated and ionized, accelerated by an electric field, deflected according to their mass and detected in Faraday cups. The measurement was performed in static mode and the $^{143}Nd/^{144}Nd$ ratios were normalized using the $^{146/144}Nd$ ratio (reference value of 0.7219) to correct for the mass fractionation of the instrument using exponential fractionation law.

Data quality was monitored by analyzing 39 Rennes standards and 15 La Jolla standards during the measurement sessions of our PANDORA samples. The resulting standard average $^{143}Nd/^{144}Nd$ values were 0.511962 ± 0.000012 and 0.511849 ± 0.000009 (2σ), respectively. The reference values of these standards being 0.511961 ± 0.00001 for Rennes (Chauvel and Blichert-Toft, 2001) and 0.511858 ± 0.000007 for La Jolla (Lugmair et al., 1975), PANDORA sample $^{143}Nd/^{144}Nd$ measurements were corrected for a machine bias of 0.000006. The internal precision of each TIMS analysis were calculated automatically by the MatSpec software (Finnigan®) and the measurements were reported with 2σ error bar. When the internal measured precision was worse than the external one, its value was assigned to the analyzed Nd-IC. When it was better, the external precision was applied. The consistency of the Nd-IC data was validated by replicate measurements: six filtered samples from station 73 at 1,650 m, two non-filtered from station 73 at 1,650 m and three non-filtered samples from station 82 at 1,200 m. The resulting ε_{Nd} values were consistent within 9% uncertainty. Total blank value was 6 pg (n = 6),

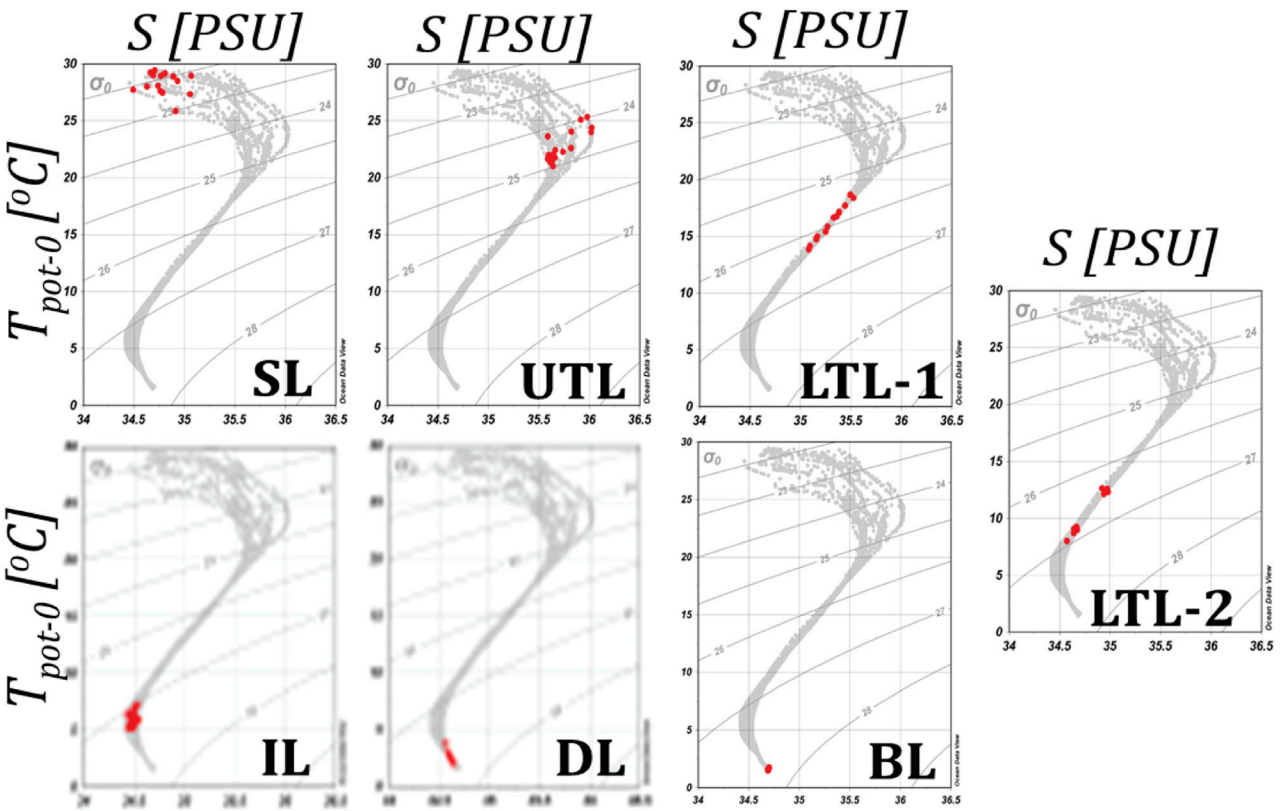

FIGURE 3 | Potential temperature (θ) versus salinity (S) plots for the PANDORA stations (grey curves). Samples collected within each specific layer described in **section 2.3** are identified by red dots. Potential density anomaly contours are shown as solid grey lines. SL, surface layer; UTL, upper thermocline layer; LTL-1, lower thermocline layer–upper extent; LTL-2, lower thermocline layer–lower extent; IL, intermediate layer; DL, deep layer; BL, bottom layer.

identified by applying similar analytical protocol to blank matrix (distilled water) and then measured by ICP/MS, representing less than 1% of the signal.

2.3 Comparison of Our Nd-IC Signatures With Preceding Studies and Data Validation

Grenier et al. (2013) analyzed samples at stations located in the North Caledonian Jet core (Coral Sea, station Flusec 43- August 2007), at the entrance of the Solomon Sea (Flusec-22, August 2007) and in Vitiaz Strait (EUC-Fe 30, September 2006), allowing us to compare our data with their published values (**Figure 2**; see **Figure 1** for station locations). Comparisons of the ε_{Nd} values between these studies were made along isopycnal ranges.

An excellent agreement is observed between the ε_{Nd} values obtained in this work and Grenier et al. (2013)'s results (**Figure 2**), reinforcing the reliability of the new dataset presented here. The only slight difference (±0.2) is observed in the surface layer of Vitiaz Strait. Such small Nd-IC variations at different sampling times likely reflect surface water natural variability, either due to variable external sources or highly variable circulation. This is discussed in the following section.

Note that, although conducted in the same laboratory, Grenier did not follow the same protocol and used older mass spectrometers (both ICP-MS and TIMS). Since there is no cross over station in this area, this good comparison was an important criterion to validate our data. Based on this quality report, these Nd-IC measurements were validated by the GEOTRACES Standard and Intercalibration committee and deposited in the 2021 GEOTRACES Intermediate Data Product (https://geotraces-portal.sedoo.fr/pi/).

2.4 Regional Hydrography of the Study Area

The detailed hydrological properties of the waters flowing from the Coral Sea into the Solomon Sea were presented in Pham et al. (2019). The general circulation scheme, current names and locations of the different stations used in this study are provided in **Figure 1**. The hydrological properties of the different layers are recalled as T-S diagrams in **Figure 3**, and are used to identify the following layers and water masses, which have different origins, pathways, and properties:

(a) Surface Layer (SL) ($\sigma_\theta \leq 24.3$ kg/m^3): Tropical Surface Water (TSW) is dominant in this layer from the northern subtropical front to the equator. In the Solomon Sea, this water mass is characterized by high temperature (~28.2°C) and low salinity (~34.5) due to the intense solar radiation and precipitation (Delcroix et al., 2014).

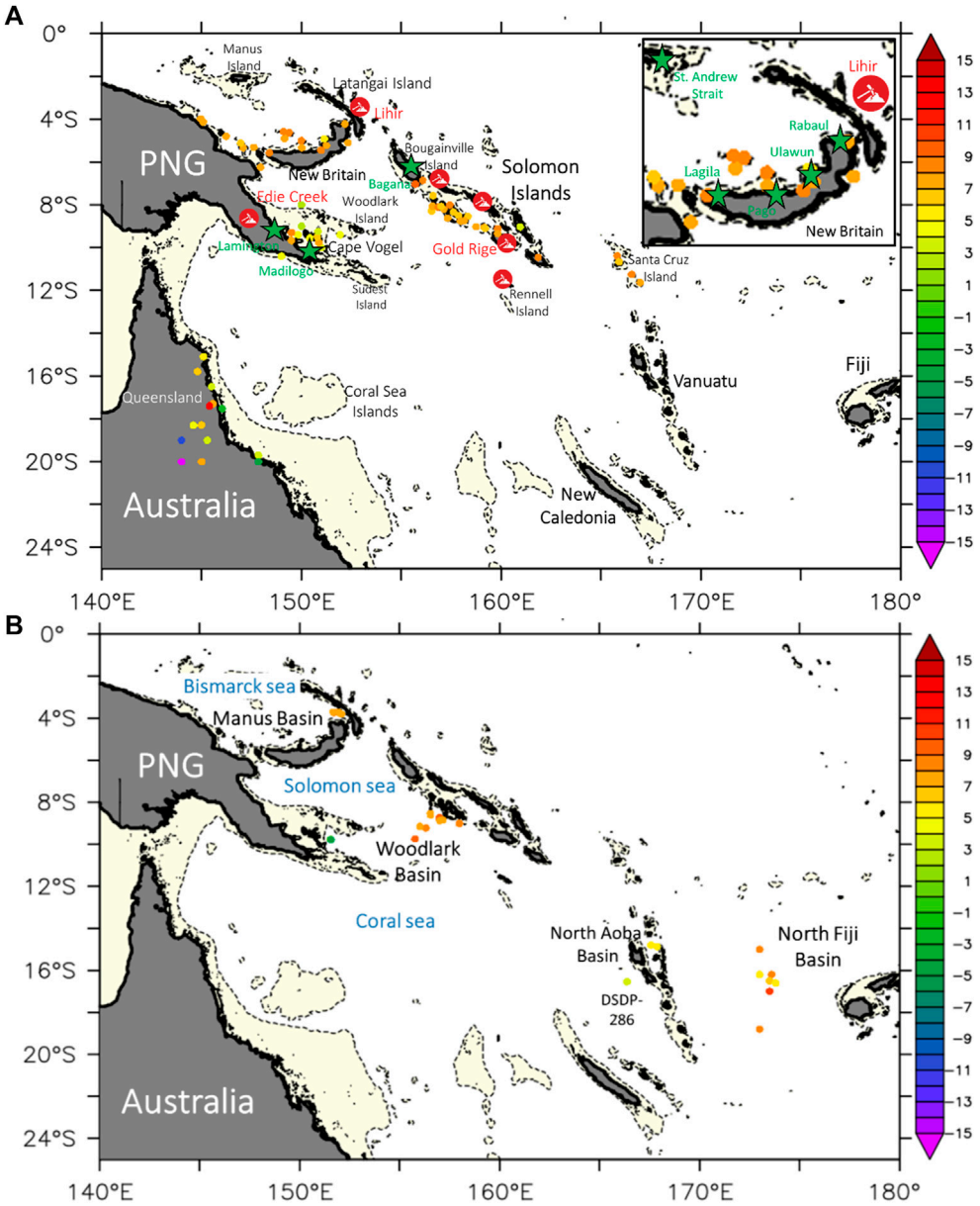

FIGURE 4 | εNd of samples of: **(A)** rocks and continent material extracted from the geochemical dataset EarthChem (http://www.earthchem.org). The areas where the bathymetry is shallower than 1,000 m depth are colored in light yellow. Green stars indicate the location of active volcanoes; their name is written beside in green. Mine locations are identified on the map by red pixel icon (Data from PNG Chamber of Mines and Petrolium, http://pngchamberminpet.com.pg/ our-resource-industry/ mining). **(B)** surface sediments collected in different basins from Fiji to the north of New Britain Island. Data are from the EarthChem portal (http://www.earthchem.org). The bathymetry shallower than 2,000 m is colored in light yellow.

(b) Thermocline layer (TL): this layer displays significant temperature and salinity gradients and includes several water masses. It can be divided into two sublayers: the upper thermocline layer (σ_θ = 24.3 – 25.3 kg/m^3) and the lower thermocline layer (σ_θ = 25.3 – 26.9 kg/m^3). The latter can also be subdivided into two extents, which correspond to the Upper and Lower extents of the lower TL.

Upper TL (*UTL*, σ_θ = 24.3 – 25.3 kg/m^3): The South Pacific Tropical Water (SPTW) flows in the upper thermocline layer (Tsuchiya et al., 1989; Qu and Lindstrom, 2002). Originating from the subtropical high evaporation area in the southeastern Pacific, this water mass is characterized by high salinity (~35.7) and low oxygen content (~141 μmol/kg; Tomczak and Hao 1989; Tsuchiya et al., 1989; Tomczak and Godfrey 2003; Kessler and Cravatte 2013b).

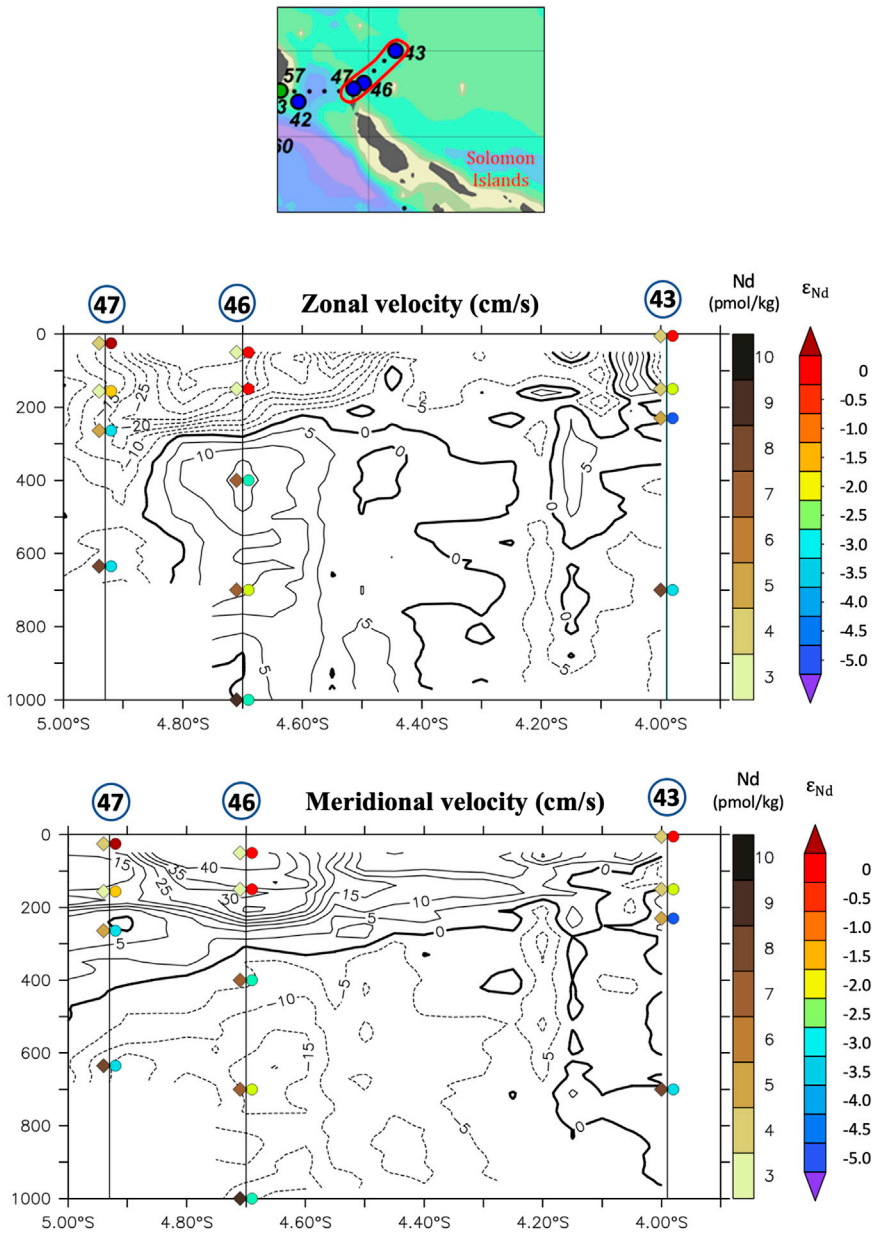

FIGURE 5 | Zonal (top) and meridional (bottom) S-ADCP velocity sections from station 43 to station 47 (Germineaud et al., 2016; Cravatte et al., 2011) overlaid with vertical profiles of εNd and Nd concentrations. Yellow color indicates positive current value, representing northward and eastward directions. values and Nd concentrations are reported on the sections by black and red numbers, respectively. Note that the currents here are dominated by tidal variability at semi-diurnal periods, and reverse

Lower TL - Upper extent (*LTL-1*, σ_θ = 25.3 – 26.4 kg/m^3): The upper extent of the lower thermocline is composed of the Western South Pacific Central Water (WSPCW). This water displays thermostat characteristics (Tsuchiya, 1981; Qu et al., 2008; Grenier et al., 2014) and a very loose stratification at about 300 m depth (~ σ_θ = 26.0 kg/m^3, Tomczak and Hao, 1989; Tomczak and Godfrey, 2003).

Lower TL - Lower extent (*LTL-2*, σ_θ = 26.4 – 26.9 kg/m^3): Underneath the WSPCW flows, we find the Subantarctic Mode Water SAMW (σ_θ = 26.5 – 26.9 kg/m^3, McCartney, 1979; Grenier et al., 2011). This water mass is characterized by a low salinity (~34.5) and high oxygen (~175 µmol/kg; Qu et al., 2009).

(c) Intermediate layer (IL, σ_θ = 26.9 – 27.4 kg/m^3): the intermediate layer of the Solomon Sea is a mixture of Antarctic Intermediate Water (AAIW) entering the sea through its southern entrance, characterized by a maximum in oxygen (~180 kg/m^3) and minimum in salinity (~34.5), and of Equatorial Pacific Intermediate Water (EqPIW), with low oxygen (~115 µmol/kg), coming

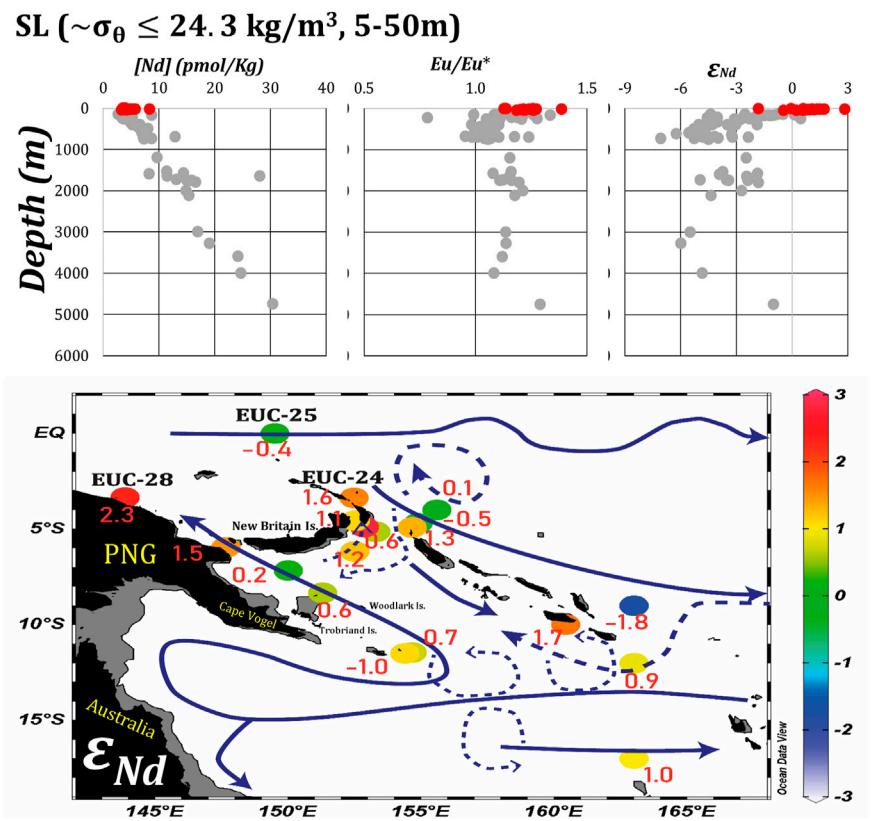

FIGURE 6 | Properties and main circulation scheme of the surface waters (5-50 m). Top: [Nd], Eu anomaly and εNd vertical profiles for PANDORA stations (grey dots); surface layer samples are identified by red dots. Bottom: εNd data of the surface layer (5-50 m). Main currents are determined from (Ceccarelli et al., 2013) and represented by continuous dark blue arrows. In addition, current anomalies observed during PANDORA and related mesoscale features are represented by dashed arrows. The bathymetry shallower than 50 m is colored in dark grey.

from the eastern Equatorial Pacific and entering through the Solomon Strait (Bostock et al., 2010; Germineaud et al., 2016; Pham et al., 2019).

(d) Deep layer (DL, $\sigma_\theta = 27.4 - 27.65$ kg/m^3): The Upper Circumpolar Deep Water (UCDW) dominates this layer (Orsi and Nowlin, 1995; Sokolov and Rintoul, 2000; Grenier et al., 2013; Germineaud, 2016). UCDW is characterized by a high nutrient signature (Warren, 1973) and a pronounced oxygen minimum (Talley, 2007).

(e) Bottom layer (BL, $\sigma_\theta \geq 27.65$ kg/m^3): The Lower Circumpolar Deep Water (LCDW) is the main water mass identified in this layer (Reid, 1997; Tsimplis et al., 1998; Kawabe and Fujio, 2010). It is characterized by a salinity maximum reaching 34.72–34.73 and a decrease of its silicate content when compared to the UCDW (Orsi et al., 1999). From the known topography, the Solomon Sea is closed below 3,500 m, separated from the surrounding basins by islands and sills. However, Lower Circumpolar Deep Water imprint was clearly identified in the Solomon Sea profiles, with an unexpected oxygen concentration increase with depth, which suggests that the densest part of the UCDW entering the Solomon Sea is likely influenced by LCDW properties (Germineaud et al., 2021).

2.5 Geochemical Setting and Nd-IC Signal of the Potential Lithogenic Sources

Geographical maps showing the ε_{Nd} values of the different continents were published by Jeandel et al. (2007), Robinson et al. (2021) and more regionally by Grenier et al. (2013). However, none of these maps are detailed enough for our local study. Here, published data on rocks, beach sand and detrital lithogenic particles have been extracted from 28 geological studies surrounding the studied area using the EarthChem portal and reported in **Figure 4A** (http://www.earthchem.org; Jeandel et al., 2007; Robinson et al., 2021).

Volcanoes, that are potential sources of fresh basaltic dusts, extracted from the Global Volcanism Program are also reported in **Figure 4A** (http://volcano.si.edu/gvpvotw.cfm). The most important gold, nickel or bauxite mines are located on the following islands: Papua New Guinea (Eddie Creek), Solomon (Choiseul and Santa Barbara), Guadalcanal, Rennel and finally Lihir that hosts one of the biggest goldmines of the world

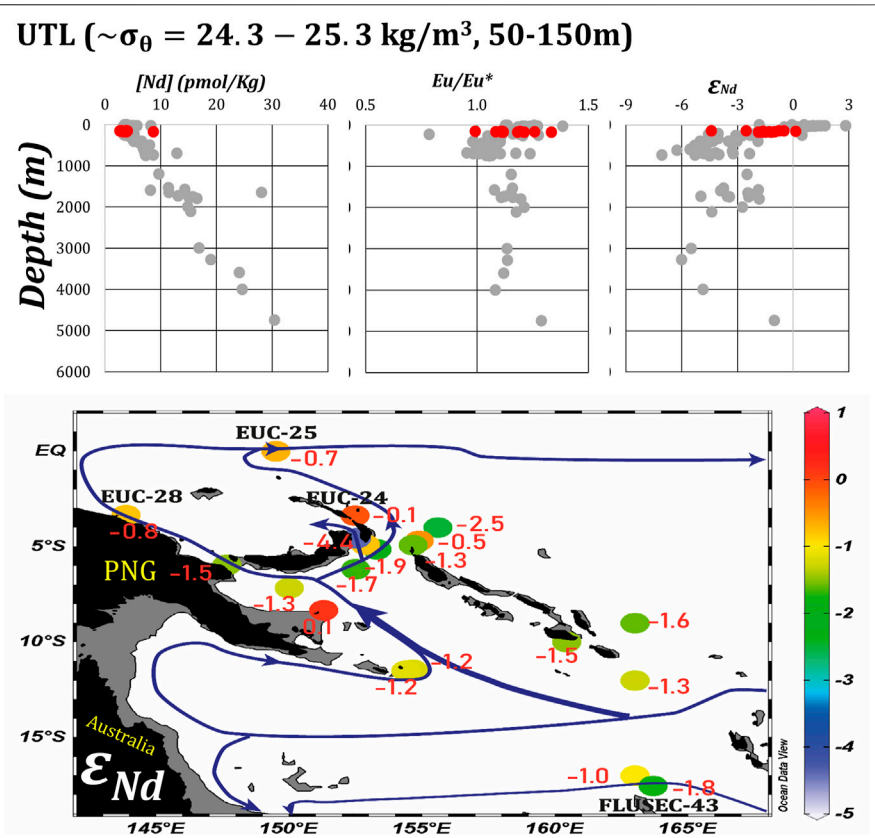

FIGURE 7 | As **Figure 6** for the Upper Thermocline Layer (24–25.3 kg/m^3). The bathymetry shallower than 200 m is colored in dark grey.

(**Figure 4A**). By accelerating the weathering, this anthropogenic activity could also modify the Nd parameters (concentration and IC) of the seawater. The sediment Nd-IC data are still very scarce in this remote area: those we could have identified are reported in **Figure 4B**. From the north Fiji Basin to the eastern part of Manus Basin, high radiogenic signals are have identified, the highest ε_{Nd} values reaching +10 (Briqueu et al., 1994; Nohara et al., 1994; Kamenetsky et al., 2001; Hegner and Smith, 1992; Beier et al., 2015). At the southern entrance of the Solomon Sea, sediments of the Woodlark Basin show radiogenic values close to the Solomon Islands (ε_{Nd} ranging between +7.3 and +9.4) while negative values (down to −4.8) are observed at the western end of the section, in the eastern Papua New Guinea's bay (Chadwick et al., 2009; Speckbacher et al., 2012).

Most of the ε_{Nd} data reported in **Figures 4A,B** display very radiogenic signature, in agreement with the back-arc tectonic and volcanic structures of the studied area. However, some specific areas display negative ε_{Nd} values (Australian and south Papua New Guinea coasts essentially). The Australian eastern coast appears as a patchwork of different lithogenic materials signed with both positive and negative ε_{Nd} values (Rudnick et al., 1986; Ewart et al., 1988; Allen, 2000; Zhang, 2001; Handler et al., 2005). Consequently, the coastal region extending from −18°S to −16°S results of interlacing between Paleozoic and Mesozoic materials (e.g., felsic dacite, lherzolite and granulite), which lead to fluctuating ε_{Nd} values, ranging from −18 to +5. South of PNG, the observed negative values likely reflect deposits of metamorphic materials outcropping on a large part of Cape Vogel. (**Figure 4A**; http://exploringtheearth.com/2018/04/30/exploration-papua-new-guinea/pnggeology/).

3 RESULTS AND DISCUSSION

3.1 Nd Concentration and Isotopic Composition

Neodymium concentration ([Nd]) and Eu anomaly (Eu/Eu*) are taken from Pham et al. (2019). The calculation of the europium anomaly is derived from the gadolinium anomaly expression of Bau et al. (1996); it compares the measured Eu concentration to the neighboring REE Sm and Dy, all normalized to PAAS (Post-Archean Australian Average Shale)[1]. A positive anomaly (>1.0) suggests an imprint of basaltic material in the Solomon Sea, the highest positive values corresponding to the most recent inputs. Neodymium isotopic composition signatures are reported in **Table 1**, within ±2σ. In the following, only the significant variations, i.e., those beyond analytical precision, are

[1] $\frac{Eu}{Eu^*} = \frac{4 \times [Eu]_n}{3[Sm]_n + [Dy]_n}$

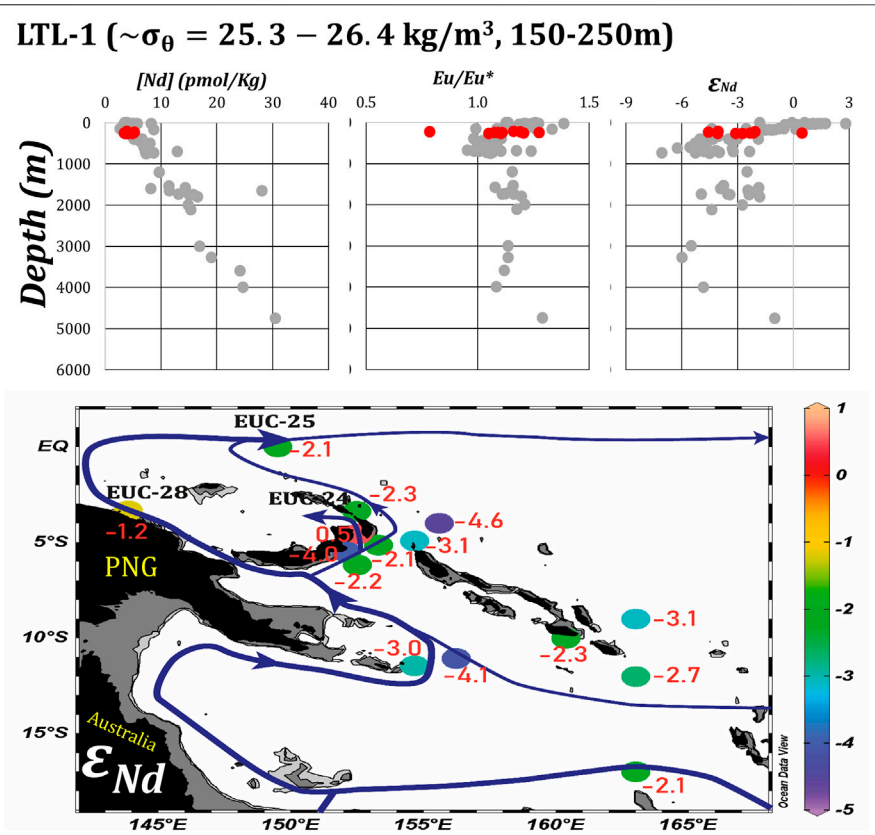

FIGURE 8 | As **Figure 7** for the Lower Thermocline -Upper extent (25.3–26.4 kg/m^3). The bathymetry shallower than 200 m is colored in dark grey and in light grey when shallower than 500 m.

discussed. Data are first discussed qualitatively according to the water mass distribution outlined in **section 3.1** (**Figures 5–11**). Where possible, land-ocean exchanges are quantified and discussed in **section 3.2**. The station locations are mentioned in **Figure 1**.

3.1.1 Surface Layer

Surface waters are characterized by a pronounced radiogenic signal (Nd-IC varying from −2 to +3) and positive Eu anomalies up to 1.3.

At the entrance of the Solomon Sea (station 34; **Figure 1**), Nd-IC and [Nd] of the surface waters display the same values (~ ε_{Nd} = +1.0, [Nd] = 4.5 pmol/kg) as in the center of the Coral Sea (station 10; see **Figure 1** for location). Closer to the Papua New Guinea's coast, more negative ε_{Nd} values are found at station 36 (ε_{Nd} = −1) and [Nd] are twice as high, reaching 8.2 pmol/kg. These values could result from: i) a modification of the water signature while flowing along the Australian coast characterized by unradiogenic fields, ii) recent local inputs from the extreme southern tip of the PNG (**Figure 4A**). However, the lack of precise Nd-IC of this PNG extreme tip prevents us from any further conclusion.

Surface waters in the three northern straits are more radiogenic than in the southern entrance, the most radiogenic values (~ ε_{Nd} = +1.3) are observed in the eastern St. George's Channel and Solomon Strait, where the surface waters are entering the Solomon Sea. This likely reflects inputs from radiogenic active volcanoes located on New Britain Island or the influence of Lihir mine (**Figure 4A**, Schuth et al., 2004; Schuth et al., 2009). Within the Solomon Sea, ε_{Nd} increases between station 71 (~ ε_{Nd} = +0.6; Trobriand-Woodlark islands) and Vitiaz Strait (~ ε_{Nd} = +1.5) while [Nd] remains relatively constant (~4 pmol/kg). Further east, a high ε_{Nd} value (+2.8) is observed at the sea surface of station 53 (**Figure 1**) while upstream surface waters are less radiogenic (ε_{Nd} = +1.6, station EUC-Fe 24; Grenier et al., 2013) and [Nd] does not significantly change between these two stations. Finally, in the southeast of the Solomon Sea, surface waters collected downstream the Indispensable Strait (stations 20 and 21; ε_{Nd} = +1.7, [Nd] = 4.7 pmol/kg) show an increase of ε_{Nd} and a slight Nd enrichment compared to the waters sampled upstream the strait (station 13; ε_{Nd} = −1.8 [Nd] = 3.9 pmol/kg). Surface water modifications at these three sites could reflect BE processes along Cape Vogel (station 71-Vitiaz, **Figure 11**), and the New Ireland's coast (station 53) or within the Indispensable Strait (station 13–21). In all cases, high radiogenic material here could come from regular weathering or wastes discharged from extracting activities (Cape Vogel, Lihir Mine and Gold exploitation on Guadalcanal respectively; **Figure 4A**).

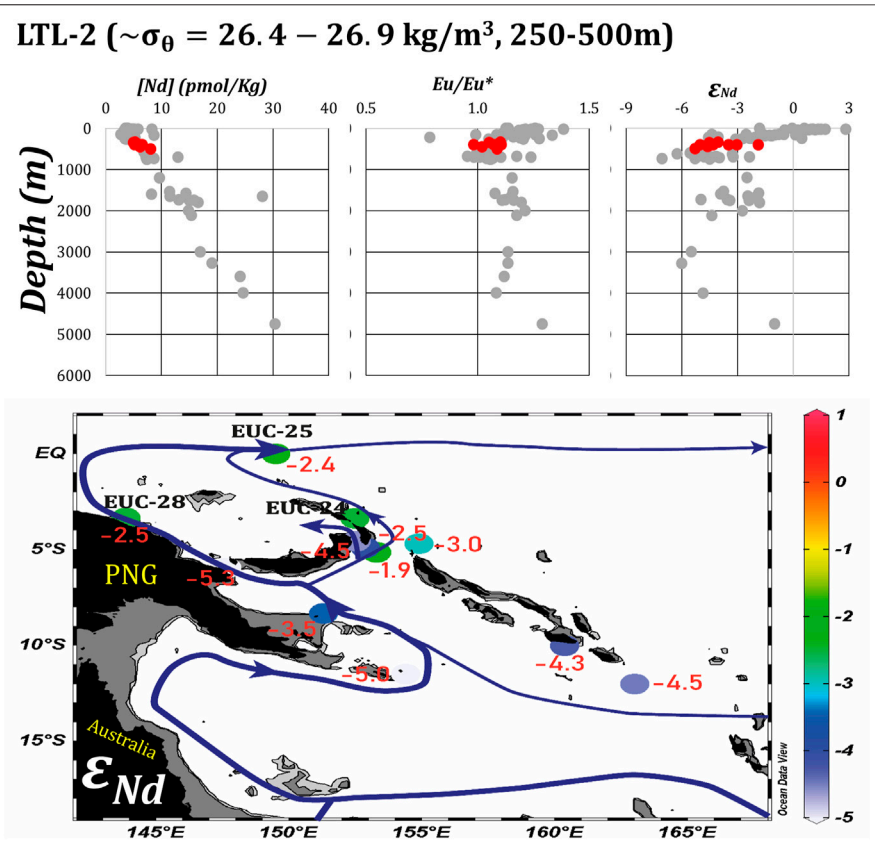

FIGURE 9 | As **Figure 8** for the Lower Thermocline-Lower extent (26.4–26.9 kg/m^3). The bathymetry shallower than 200 m is colored in dark grey and in light grey when shallower than 500 m.

At the eastern end of the Solomon Strait (stations 46 and 47 in **Figure 1**), ε_{Nd} and [Nd] decrease from + 1.3 and 4.4 pmol/kg at station 47 to −0.5 and 3.3 pmol/kg at station 46 respectively, despite the close proximity of the two stations (~20 nautical miles). Actually, station 46 seems to be under the influence of colder water brought by a small oceanic mesoscale eddy located at 4.8°S. It is noted that this eddy also affects the thermocline layer below (see **Figure 11**).

3.1.2 Thermocline Layers

Nd isotopic signatures are reported in **Figures 7–9** for the Upper and Lower Thermocline layers (upper and lower extents), respectively.

Vertical distribution: these layers can be distinguished by their different average Nd-ICs. In the upper thermocline layer (**Figure 7**), ε_{Nd} values range between −1.9 and −0.8. Below 150 m, the upper extent of the lower thermocline layer (**Figure 8**) is characterized by values slightly less radiogenic, ranging from −4.1 to −2. Finally, the lower extent of this layer displays ε_{Nd} values slightly less radiogenic again ranging between −5.3 and −2.4. These different ranges of values likely reflect the different origins and pathways followed by the currents transporting these layers, including their potential contact with fields of different geochemical characteristics. Water mass flowing in the upper thermocline layer entering the Solomon Sea are more negative at station 29 (ε_{Nd} = −4.1) than at the upstream station 10 in the eastern Coral Sea (ε_{Nd} = −2.7), which could reflect an imprint of the negative sources characterizing the Australian coast (**Figure 4A**). While waters are relatively radiogenic (~ ε_{Nd} = −2.5) in the upper extent of the lower thermocline layer due to its Tasman Sea origin, the SubAntartic Mode Water of southern origin is more negative (~ ε_{Nd} = −4.5) in the lower extent of the lower thermocline layer.

Horizontal distribution: each layer is characterized by a south-north increase of the ε_{Nd} values, although these fluctuations remain modest (~2 ε_{Nd} units). Meanwhile, Nd concentrations also barely vary (4–5 pmol/kg), as reported in **Figures 7–9**. Inside the Solomon Sea, these south-north IC gradients likely reflect a general modification of the waters signatures by the radiogenic fields surrounding this area due to BE processes. This is well illustrated by the ε_{Nd} values of the lower thermocline waters (**Figure 8**), which increase from ε_{Nd} = −4.1 in the south (station 29) to approximately −2 in the north (stations 42 and 60) while the Nd concentrations do not change, leading us to suspect occurrence of BE at the scale of the Solomon Sea for this layer. However, at a regional scale, more radical and rapid changes of Nd-IC are observed. In the upper extent layer still (**Figure 8**), station 57 is marked by a significant increase of Nd-IC (ε_{Nd} = + 0.5) in the middle of the St. George's Channel compared to station 58 (ε_{Nd} = −4.0). This high value without clear [Nd] changes likely reflect local BE processes. From the inverse

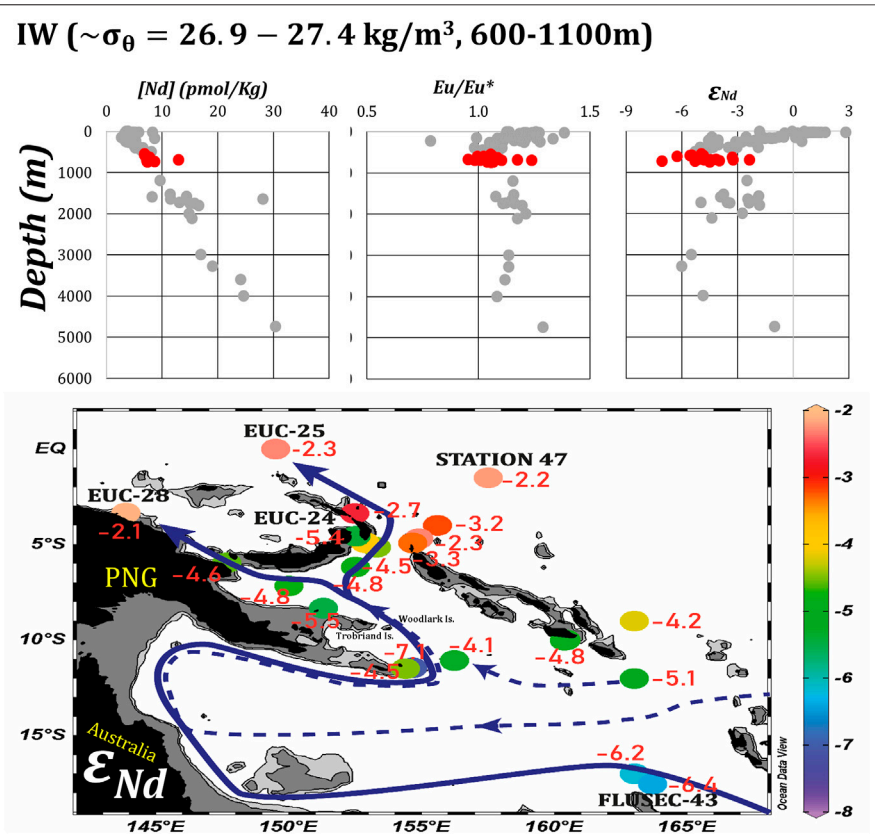

FIGURE 10 | As **Figure 9** for the intermediate layer (26.9–27.4 kg/m^3). The bathymetry shallower than 500 m is colored in dark grey and in light grey when shallower than 1000 m.

modelling study of Germineaud et al. (2016), it takes about 3–4 days to this layer to reach station 57 from station 58. This reflects that boundary exchange is very rapid along the New Britain Island margin and strait. Following the current vein transporting the lower extent of the lower thermocline (LTL-2, eastern branch), variations of Nd-IC between station 71 (ε_{Nd} = −3.5, **Figure 7**) and 42 (ε_{Nd} = −1.9, **Figure 8**) while Nd concentration remains the same can again only be explained if BE processes are invoked.

Finally, more radiogenic water is found after passing through the Indispensable Strait (station 21; ε_{Nd} = −2.3), compared to station 13 (ε_{Nd} = −3.1, **Figure 7**), this time accompanied by a slight Nd concentration increase, which can also indicate BE occurrence, with a net input larger than the removal scavenging effect.

3.1.3 Intermediate Layer

The two water masses identified in this layer (600–1,100 m) are the Antarctic Intermediate Water (AAIW) and the Equatorial Pacific Intermediate Water (EqPIW; **section 2.3**). The Nd-IC ranges from approximately −5.0 at the entrance of the Coral Sea to up to the contrasting value of −2.3 north of the Solomon Sea. The [Nd] however, stays relatively constant (~8 pmol/kg; **Figure 9**).

In the Coral Sea, the AAIW is transported by the NCJ from North Caledonia to the South West entrance of the Solomon Sea, flowing close to the unradiogenic Queensland coast. This likely explains why the water is slightly more negative at station 34 than at station 4 or even FLUSEC-43; **Figure 4A**). The higher ε_{Nd} values measured at stations 29 and 36 (~ ε_{Nd} = −4.3) compared to those at station 10 (ε_{Nd} = −5.1) could reflect the impact of sediments, weathered from the Southeast of the PNG and deposited on the shelf around station 36 (**Figure 4B**).

Waters are slightly more radiogenic at station 71 (ε_{Nd} = −5.5) than upstream (station 36, ε_{Nd} = −7.1) with quite similar [Nd] (~8 pmol/kg). Two possible processes can explain these results: i) intermediate water properties found at station 71 may result from a mixing between waters found at the stations 29 and 34. However, the differences in current velocity and pathway of this layer prevent this mixing (see **Figure 4A** of Germineaud et al., 2016); ii) BE processes are at play again, characterized by Nd exchanges with external radiogenic (~ ε_{Nd} = −1 *to* + 5) sources from the bottom of the western Woodlark basin (**Figure 4B**).

From the Solomon Sea to the St. George's Channel and Vitiaz Strait, ε_{Nd} values of IW are roughly comparable to what is observed at the southern entrance (from −5.5 to −4.5). This stable Nd-IC signal is also observed at the station 42 (ε_{Nd} = −4.5), located in the western part of the Solomon Strait. In an opposite way, a significant ε_{Nd} increase is observed in the northeastern part of the Solomon Strait (from −3.3 at station 47 to −2.3 at station 46), likely

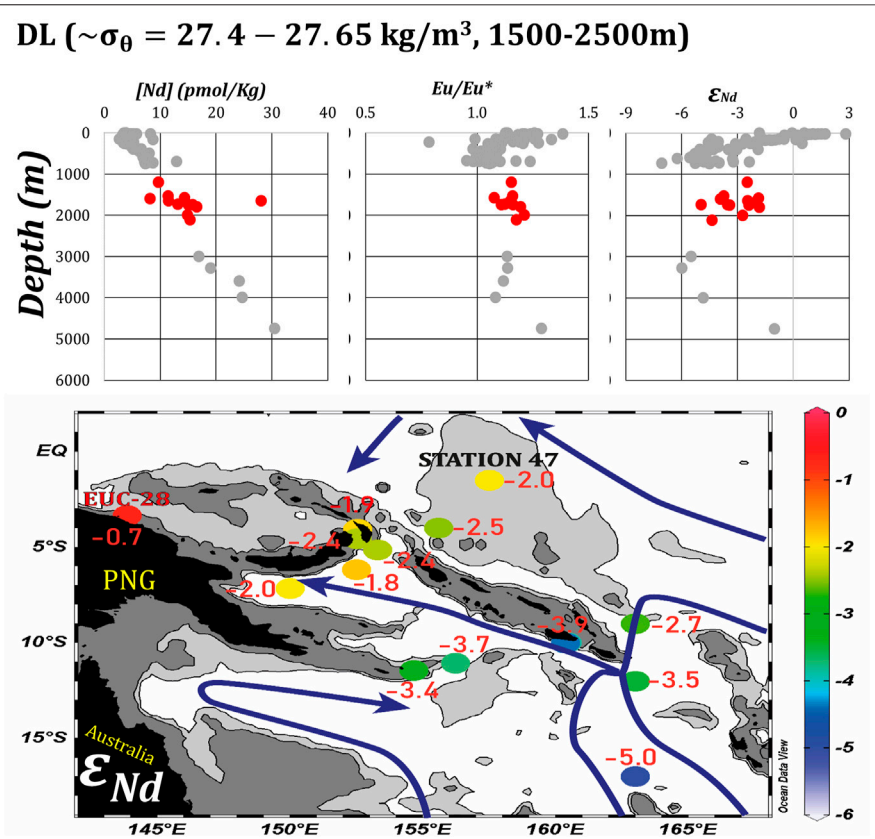

FIGURE 11 | As **Figure 10** for the deep layer (27.4–27.65 kg/m^3). The bathymetry shallower than 1500m m is colored in dark grey and in light grey when shallower than 2500 m.

reflecting the mixing between the AAIW and EqPIW, identified as very radiogenic (Bostock et al., 2010; Grenier et al., 2013). Northeast of the strait, station 46 (ε_{Nd} = −2.3) is again different from neighbouring stations, but at this depth it displays a more radiogenic value than in the northern Coral Sea (ε_{Nd} = −4.1). This suggests an intrusion of water coming from the equator, probably still a consequence of the mesoscale eddy mentioned above (**Figure 12**). This influence should end between station 46 and 13 since a clear AAIW signature (~ ε_{Nd} = −4.2) is observed at the latter.

3.1.4 Deep Layer

At these depths (1,500–2,500 m), the bathymetry becomes a strong constraint for the circulation, motivating a detailed report of the submarine terrain in **Figures 10**, **11**. A close look at this bathymetry and the water mass properties allowed establishing that UCDW enters the Solomon Sea via two narrow passages at 156°E and 162°E along the southern section (Germineaud et al., 2021). It then exits through St. George's channel and Solomon strait only, since Vitiaz strait is blocked by the depth of the sill (980 m). Along the south-north pathway of the UCDW (i.e. from the Solomon Sea entrance to the two remaining exits), an increase of both the Nd-IC and [Nd] is observed (**Figure 10**). These parameters vary from ~ ε_{Nd} = −3.6 and [Nd]= 11 pmol/kg in the south to ~ ε_{Nd} = −2.0 and [Nd]= 14 pmol/kg in the north. These variations reflect inputs of radiogenic Nd. Thus, BE processes are suspected to occur at the scale of the Solomon Sea for this layer.

3.1.5 Bottom Layer

Only three samples characterize the LCDW but they are worth to be discussed, considering how poorly documented this water mass. From 3,500 m down to the bottom, the Nd-IC signal of LCDW is more negative outside the Solomon Sea with values around −6. This contrasts with the radiogenic value of −1.0 observed at station 60 in the core of the Solomon Sea. [Nd] also increases from 22 pmol/kg outside the Solomon Sea to 30 pmol/kg at the bottom of station 60. In addition, the oxygen profile of station 60 suggests that relatively ventilated waters are penetrating the Solomon Sea from the south (Ganachaud et al., 2017; Pham et al., 2019). Germineaud et al. (2021) suggested that the lower part of the UCDW can imprint the LCDW and generate its O_2-rich signature within the Solomon Sea. However, UCDW ε_{Nd} of −3.4 to −3.9 could not explain the observed LCDW signature change from −6.0 to −1.0. Thus, a process might modify the Nd parameters of the LCDW as it enters the Solomon Sea through the complex topography of the southern sill. We hypothesize that inputs from the sediment deposited on the bottom Woodlark basin slope occur (ε_{Nd} from −4.8 to +9.4; **Figure 4B** and **section 2.4**, Chadwick et al., 2009; Speckbacher et al., 2012). Boundary exchange likely takes place

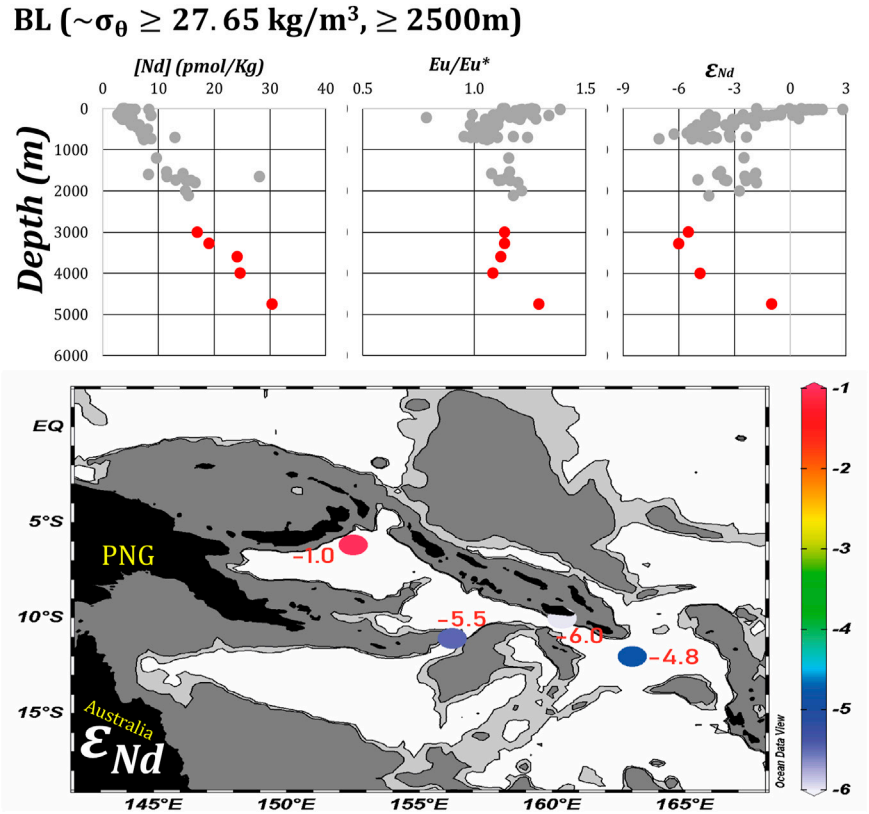

FIGURE 12 | As **Figure 11** for the bottom layer (≥27.65 kg/m3). The bathymetry shallower than 2500 m is colored in dark grey and in light grey when shallower than 3000 m.

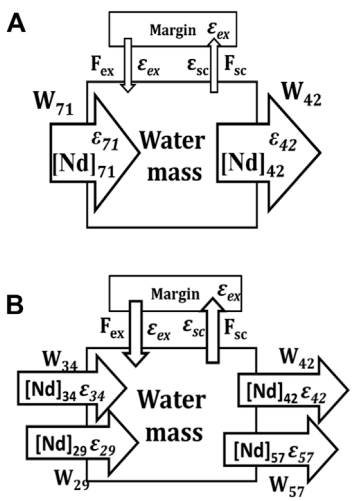

FIGURE 13 | Representations of the box models used to calculate the Nd exchanged fluxes at the land-ocean interface for **(A)** local application (LTL-2) and **(B)** the whole Solomon Sea (DL). Note that for the latter, Vitiaz Strait is closed.

here with both increase of ε_{Nd} and [Nd], reflecting greater Nd release from the margin and/or the bottom sediments than scavenging within the water column.

3.2 Quantifying the Boundary Exchange Process

The evolution of the Nd parameters along the different layers reveals different inputs, either very local -as for example in the Indispensable Strait-or on the scale of the whole Solomon Sea -as illustrated by the changes affecting the deep layer. Boundary Exchange quantification requires the following parameters: [Nd], Nd-IC and the water transport of the considered layer. The box model calculations proposed in the following are restricted to two layers -lower extent of lower thermocline layer (LTL-2) and deep layer (DL)- for which we could gather the three parameter values for each entrance and exit sections. We drew two box models, one for the local scale, applied to the LTL-2 and another one for the Solomon Sea scale, applied to the DL (**Figure 13**). All the water mass transports (W) are estimated by Germineaud et al. (2016) and extended to deeper layers as in Pham et al. (2019). Regarding the sediment taken as external source, we are aware that the sediment comprise various phases (e.g., carbonate-

TABLE 2 | Fluxes calculated from local-LLTW and PANDORA-UCDW box models.

Layer		WM transport (Sv)	Nd conc. (pmol/kg)	ε_{Nd}	ε_{sc}	ε_{ex}	Net flux-$F_{net\ total}$ T (Nd)/yr	Scavenging flux- F_{sc} T (Nd)/yr	External flux - F_{ex} T (Nd)/yr
LTW-2 (σ_θ = 26.4–26.9 kg/m^3)	Enter	W_{71}: 1.7	0.8 ± 0.0	−3.5 ± 0.2	−1.9	+5.1	6.1 ± 1.7	1.8 ± 2.3	7.9 ± 2.0
	Exit	W_{42}: 1.7	0.9 ± 0.0	−1.9 ± 0.3					
UCDW-Upper extent (σ_θ = 27.4–27.65 kg/m^3)	Enter	W_{29}: 4.5	1.5 ± 0.2	−3.9 ± 0.2	−2.3	+5.1	68 ± 31	−24 ± 26	44 ± 18
		W_{34}: 1.0	2.0 ± 0.1	−3.5 ± 0.2					
	Exit	W_{42}: 4.0	2.0 ± 0.1	−2.2 ± 0.2					
		W_{57}: 1.5	1.7 ± 0.0	−2.5 ± 0.2					
UCDW- Lower extent (σ_θ = 27.65–27.76 kg/m^3)	Enter	W_{29}: 3.0	2.4 ± 0.4	−3.8 ± 0.2	−2.1	+5.1	37 ± 39	5 ± 36	42 ± 25
	Exit	W_{42}: 2.5	2.9 ± 0.4	−2.4 ± 0.5					
		W_{57}: 0.5	2.9 ± 0.0	−1.5 ± 0.2					

Entering and exiting branches of the model correspond to what was identified in ***Figure 9****. The water masses and Nd concentrations are taken from Tables 3 and 4 of Pham et al. (2019). Water mass transport were calculated with the inverse model used in Germineaud et al. (2016), following Pham et al. (2019).*

dissolved nano phases, iron oxide, volcanic material, bulk detrital) that are not dissolving at the same rate. In addition, different phases might be characterized by different Nd isotopic signatures (Wilson et al., 2013). This complexity makes it difficult to estimate the fluxes of elements released by the sediments. Yet, the scarcity of the data characterizing the Solomon Sea sediments led us to consider them homogeneous (made of a majority of basalts), with a unique ε_{Nd} value (ε_{Nd} = +5.1, taken as ε_{sc} in the following), averaged on the base of the EarthChem compilation. This value very similar to the one obtained when averaging the signatures of the fields surrounding the Solomon Sea, which strengthens its representativity. Calculations are made assuming steady state (i.e., inputs and outputs are balanced) and assuming that no diapycnal mixing occurs within the defined boxes.

3.2.1 Box Model for Lower Thermocline Layer-Lower Extend

The eastern branch of the LTL-2 water is likely impacted by BE processes, from station 71 (ε_{Nd} = −3.5) to 42 (ε_{Nd} = −1.9). The exchanged fluxes are quantified considering the water layer as defined by Germineaud et al. (2016) and using the box model described in **Figure 13A**. The error bars of the fluxes are estimated by propagating uncertainties. The evolution of the Nd parameters within the box follows the **Equations 1** and **2**:

$$W \times [Nd]_{71} + F_{net\,flux} = W \times [Nd]_{42} \quad (1)$$

$$W \times [Nd]_{71} \times \varepsilon_{71} + F_{ex} \times \varepsilon_{ex} - F_{sc} \times \varepsilon_{sc} = W \times [Nd]_{42} \times \varepsilon_{42} \quad (2)$$

Where:

$F_{net\ flux} = F_{ex} - F_{sc}$

F_{ex} is the external Nd flux coming from the neighbor island margin.

F_{sc} is the "scavenging" flux exported from the water mass toward the sediments due to adsorption of dissolved Nd on the particles.

W is the water transport, taken a 1.7 Sv (from the inverse model used in Germineaud et al., 2016).

$[Nd]_{71}$ and ε_{71} are the input Nd parameter values.

$[Nd]_{42}$ and ε_{42} are the output Nd parameter values

Calculation of F_{ex} and F_{sc} requires to constrain ε_{ex} and ε_{sc}, the isotopic signatures of the external source and of the scavenged particles respectively. The ε_{ex} value is taken here at +5.1 (see above). The ε_{sc} value is assumed to be similar to the exiting one (here equal to ε_{42}) following Grenier et al. (2014).

Table 2 compiles both the numerical values used in the calculations and the results. For the local box, we estimate an external flux of 7.9 ± 2.0 t(Nd)/yr and a scavenging one of 1.8 ± 2.3 t(Nd)/yr to satisfy both the [Nd] and ε_{Nd} variations, which gives a net flux of 6.1 ± 1.7 t(Nd)/yr. This net flux is consistent with the result of Pham et al. (2019), but the Nd isotopic compositions allowed us to identify the total and exchanged fluxes.

3.2.2 PANDORA Box, Applied to the Deep Layers

The significant increase of ε_{Nd} while [Nd] remains constant along the south-north pathway of the UCDW in the deep layer clearly suggests that BE processes impact this water layer. Here,

we apply a version of the 'PANDORA box model' enriched with the Nd-IC parameters to estimate the exchange intensity.

The "PANDORA box" for UCDW represented in **Figure 13B** is similar to that described in Pham et al. (2019). The striking feature here is that we have to split the calculation into two parts because the topography prevents water transport below 2,000 m at station 34. The evolution of the Nd parameters within the box follows the **Equations 3**, **4** below:

$$W_{29} \times [Nd]_{29} + W_{34} \times [Nd]_{34} + F_{net\,flex} = W_{42} \times [Nd]_{42} + W_{57} \times [Nd]_{57} \quad (3)$$

$$W_{29} \times [Nd]_{29} \times \varepsilon_{29} + W_{34} \times [Nd]_{34} \times \varepsilon_{34} + F_{ex} \times \varepsilon_{ex} - F_{sc} \times \varepsilon_{sc} = W_{42} \times [Nd]_{42} \times \varepsilon_{42} + W_{57} \times [Nd]_{57} \times \varepsilon_{57} \quad (4)$$

Where: $F_{net\ flux} = F_{ex} - F_{sc}$

F_{ex} and F_{sc}: see definition above

$[Nd]_{29}$; ε_{29} and $[Nd]_{34}$; ε_{34} represent the input Nd parameter values of station 29 and station 34, respectively.

$[Nd]_{42}$; ε_{42} and $[Nd]_{57}$; ε_{57} represent the output Nd parameter values of station 42 and station 57, respectively.

The only missing Nd parameters data are for the lower extent of UCDW (σ_θ = 27.65–27.76) at station 29. We therefore estimate these values using the neighboring stations (stations 04 and 34) due to their similarity in [Nd] and Nd-IC values (**Table 1**). The ε_{ex} is + 5.1 (see above) while. the ε_{sc} value is calculated by averaging the value of all exiting stations.

The results show similar net flux (42–43 t(Nd)/yr) for both extents of UCDW. Scavenging fluxes are affected by large error bars but they are clearly lower than the external input. The negative value estimated in the upper layer indicates that Nd desorption from the particles is required to balance the Nd concentration variation. The total net flux for the whole UCDW is 105 ± 50 t(Nd)/yr, in which external flux is 86 ± 31 t(Nd)/yr while scavenging flux is −19 ± 44 t(Nd)/yr. This net flux value is consistent with the findings of Pham et al. (2019), although better constrained (higher precision). In addition, satisfying the ε_{Nd} variation between the entrance and exit of the Solomon Sea requires a significant external input of radiogenic dissolved Nd (partly balanced by scavenging following the BE mechanism) into the DL.

3.2.3 Observed Enrichments Versus External Sources

The estimated external Nd fluxes required to change the isotopic signatures are of 7.9 ± 2.0 t(Nd)/yr in the LTL-2 and 86 ± 31 t(Nd)/yr in the DL. In this section, we compare this required input to the potential external sources for depth around 400 m (LTL-2) and beyond 2,000 m (DL).

At such depths, dust or dissolved river inputs are not likely sources because they affect the surface layer only. The weathered sediments transported by the rivers and deposited on the margins are thus considered. The only solid river discharge that could impact the Solomon Sea is brought by the mountaineous river system located at the Southeast of PNG (e.g., Fly River, Makharm River) with a total sediment discharge flux reaching 400×10^6 t/year (**Figures 5**, **6** of Milliman, 1995). Considering a Nd concentration of 32 ppm for suspended particulate matter of Fly River water (Sholkovitz, 1996; Sholkovitz et al., 1999), the resulting Nd flux is 12.8×10^3 t (Nd)/year. Knowing that only ~10% of sediment is accumulating on the adjacent shelf and less than 3% of the particles would eventually dissolve (Jeandel and Oelkers, 2015), such solid discharge could bring 346t (Nd)/year. This value is much higher than the upper limit of the flux required to enrich LTL-2 and DL. This suggests that this riverine flux brings enough material to contribute to the REE inputs in the layers for which the BE processes could be quantified. The ongoing analyses of the particles will help to further conclude.

4 CONCLUSION

Here we report the neodymium isotopic composition of seawater samples collected at 21 stations in the Coral and Solomon seas during the PANDORA cruise (July-August 2012). These data complement the REE concentration dataset reported in Pham et al. (2019). The ε_{Nd} results compare well with those published by (Grenier et al., 2013). Detailed ε_{Nd} maps of the outcropping rocks and sediments surrounding the area that could constitute external sources of chemical elements to the Solomon Sea via atmospheric dust, volcanoes, extensive weathering, and mining activity are established. Maps of the Nd-IC horizontal distributions in the different water layers help identifying variations of their composition while flowing from the Coral to the Solomon Sea. On a vertical scale, ε_{Nd} values display a clear negative excursion around the thermocline then becomes more radiogenic in the intermediate waters, less radiogenic again near 2–4 km and then the very bottom is more radiogenic. On a horizontal scale, waters exiting from the Solomon Sea show a slightly higher Nd-IC signal than at the southern entrance. The release of radiogenic ε_{Nd} by dissolution of continental margin material could explain the ε_{Nd} modification along these pathways.

Box models allow calculating those external fluxes of 7.9 ± 2.0 t(Nd)/yr and of 86 ± 31 t(Nd)/yr are required to modify the Nd isotopic signatures of part of the thermocline layer and of the deep layer respectively, the latter being mostly composed of DL. The most likely external sources explaining these changes are the sediment deposited on the margins surrounding the Solomon Sea

Contrastingly, the intermediate layer shows the imprint of the negative Nd-IC signal from AAIW that enters the Solomon Sea in the South and keeps a quasi-homogeneous Nd-IC signal across the Solomon Sea ($\sim \varepsilon_{Nd} = -4.5$) until reaching the northern exiting passages. The AAIW predominance disappears in the Solomon Strait, where mixing with EqPIW occurs, marked by a more radiogenic signature ($\sim \varepsilon_{Nd} = -2.0$).

The land-ocean processes are rapid, particularly dispersed and complex in the Solomon Sea. Indeed, many small-scale ε_{Nd} contrasts are observed between close stations at certain depths, as in the Indispensable Strait, near the PNG southern tip (e.g., between stations 34 and 36 for intermediate waters), or inside the Solomon Strait (e.g., for lower thermocline waters). A good understanding of the processes leading to these contrasts require, however, further work. Moreover, fine-scale oceanic features, as well as high-frequency variability might influence the ε_{Nd} signatures. This advocates for

further investigations of the high-frequency changes in ocean circulation and geochemical processes in the Southwest Pacific region.

DATA AVAILABILITY STATEMENT

The datasets presented in this study can be found in online repositories. The names of the repository/repositories and accession number(s) can be found in the article/supplementary material.

AUTHOR CONTRIBUTIONS

VP wrote the manuscript with major support from CJ and other supports from MG, SC, CG. VP, CJ, and MB carried out the experiment. MG and CJ conceived the original idea and performed the sampling. SC and CG helped to verify the hydrological context and provide supplementary information about deep water. Gerard Eldin helped supervise the project and provide necessary information about physical oceanography. TV encouraged VP to investigate more about fluxes.

ACKNOWLEDGMENTS

The captain, officers and crew of the R/V L'Atalante are greatly acknowledged. C. Pradoux, Stéphanie Mounic and Mathieu Benoit are thanked for their technical supports. The collaboration with SOPAC/SPC, PI-GOOS, and University of Papua New Guinea was greatly appreciated. We also acknowledge Benjamin Dupont for his volunteering help during the on-board sampling. The accomplishments were made possible through concurrent contributions of national funding agencies. The PANDORA cruise has been co-funded by NSF grant OCE1029487, and by ANR project ANR- 09-BLAN-0233-01 and INSU/LEFE project Solwara (IDAO and CYBER). All the authors whose work contributed to the database GEOTRACES are acknowledged (https://www.bodc.ac.uk/ geotraces/). The International GEOTRACES Programme is possible in part thanks to the support from the U.S. National Science Foundation (Grant OCE-1840868) to the Scientific Committee on Oceanic Research (SCOR). Our great thanks to the research team TIM at LEGOS for their support and encouragement.

REFERENCES

Abbott, A. N. (2019). A Benthic Flux from Calcareous Sediments Results in Non-Conservative Neodymium Behavior during Lateral Transport: A Study from the Tasman Sea. *Geology* 47 (4), 363–366. doi:10.1130/G45904.1

Allen, C. M. (2000). Evolution of a Post-Batholith Dike Swarm in Central Coastal Queensland, Australia: Arc-Front to Backarc? *Lithos* 51 (4), 331–349. doi:10.1016/S0024-4937(99)00068-7

Amakawa, H., Yu, T.-L., Tazoe, H., Obata, H., Gamo, T., Sano, Y., et al. (2019). Neodymium Concentration and Isotopic Composition Distributions in the Southwestern Indian Ocean and the Indian Sector of the Southern Ocean. *Chem. Geol.* 511, 190–203. doi:10.1016/j.chemgeo.2019.01.007

Arsouze, T., Dutay, J.-C., Lacan, F., and Jeandel, C. (2007). Modeling the Neodymium Isotopic Composition with a Global Ocean Circulation Model. *Chem. Geol.* 239 (1–2), 165–177. doi:10.1016/j.chemgeo.2006.12.006

Bau, M., Koschinsky, A., Bau, M., Koschinsky, A., Dulski, P., Hein, J. R., et al. (1996). Comparison of the Partitioning Behaviours of Yttrium, Rare Earth Elements, and Titanium between Hydrogenetic Marine Ferromanganese Crusts and Seawater. *Geochimica Cosmochimica Acta* 60 (10), 1709–1725. doi:10.1016/0016-7037(96)00063-4

Behrens, M. K., Pahnke, K., Cravatte, S., Marin, F., and Jeandel, C. (2020). Rare Earth Element Input and Transport in the Near-Surface Zonal Current System of the Tropical Western Pacific. *Earth Planet. Sci. Lett.* 549, 116496. doi:10.1016/j.epsl.2020.116496

Behrens, M. K., Pahnke, K., Paffrath, R., Schnetger, B., and Brumsack, H.-J. (2018a). Rare Earth Element Distributions in the West Pacific: Trace Element Sources and Conservative vs. Non-Conservative Behavior. *Earth Planet. Sci. Lett.* 486, 166–177. doi:10.1016/j.epsl.2018.01.016

Behrens, M. K., Pahnke, K., Schnetger, B., and Brumsack, H.-J. (2018b). Sources and Processes Affecting the Distribution of Dissolved Nd Isotopes and Concentrations in the West Pacific. *Geochimica Cosmochimica Acta* 222, 508–534. doi:10.1016/j.gca.2017.11.008

Beier, C., Bach, W., Turner, S., Niedermeier, D., Woodhead, J., Erzinger, J., et al. (2015). Origin of Silicic Magmas at Spreading Centres-An Example from the South East Rift, Manus Basin. *J. Petrology* 56 (2), 255–272. doi:10.1093/petrology/egu077

Bostock, H. C., Opdyke, B. N., and Williams, M. J. M. (2010). Characterising the Intermediate Depth Waters of the Pacific Ocean Using δ13C and Other Geochemical Tracers. *Deep Sea Res. Part I Oceanogr. Res. Pap.* 57 (7), 847–859. doi:10.1016/j.dsr.2010.04.005

Bouvier, A., Vervoort, J. D., and Patchett, P. J. (2008). The Lu-Hf and Sm-Nd Isotopic Composition of CHUR: Constraints from Unequilibrated Chondrites and Implications for the Bulk Composition of Terrestrial Planets. *Earth Planet. Sci. Lett.* 273 (1–2), 48–57. doi:10.1016/j.epsl.2008.06.010

Boyd, P. W., Jickells, T., Law, C. S., Blain, S., Boyle, E. A., Buesseler, K. O., et al. (2007). Mesoscale Iron Enrichment Experiments 1993-2005: Synthesis and Future Directions. *Science* 315 (5812), 612–617. doi:10.1126/science.1131669

Briqueu, L., Laporte, C., Crawford, A. J., Hasenaka, T., Baker, P. E., and Coltorti, M. (1994). "Temporal Magmatic Evolution of the Aoba Basin, Central New Hebrides Island Arc: Pb, Sr, and Nd Isotopic Evidence for the Coexistence of Two Mantle Components beneath the Arc," in Proceedings of the Ocean Drilling Program, 134 Scientific Results (Ocean Drilling Program). doi:10.2973/odp.proc.sr.134.019.1994

Chadwick, J., Perfit, M., McInnes, B., Kamenov, G., Plank, T., Jonasson, I., et al. (2009). Arc Lavas on Both Sides of a Trench: Slab Window Effects at the Solomon Islands Triple Junction, SW Pacific. *Earth Planet. Sci. Lett.* 279 (3–4), 293–302. doi:10.1016/j.epsl.2009.01.001

Chauvel, C., and Blichert-Toft, J. (2001). A Hafnium Isotope and Trace Element Perspective on Melting of the Depleted Mantle. *Earth Planet. Sci. Lett.* 190 (3–4), 137–151. doi:10.1016/S0012-821X(01)00379-X

Cravatte, S., Ganachaud, A., Duong, Q.-P., Kessler, W. S., Eldin, G., and Dutrieux, P. (2011). Observed Circulation in the Solomon Sea from SADCP Data. *Prog. Oceanogr.* 88 (1–4), 116–130. doi:10.1016/j.pocean.2010.12.015

Delcroix, T., Radenac, M. H., Cravatte, S., Alory, G., Gourdeau, L., Léger, F., et al. (2014). Sea Surface Temperature and Salinity Seasonal Changes in the Western Solomon and Bismarck Seas. *Bismarck Seas. J. Geophys. Res. Oceans* 119 (4), 2642–2657. doi:10.1002/2013JC009733

Elderfield, H., Bacon, M. P., Liss, P. S., Whitfield, M., and Burton, J. D. (1988). The Oceanic Chemistry of the Rare-Earth Elements. *Phil. Trans. R. Soc. Lond. A* 325 (1583), 105–126. doi:10.1098/rsta.1988.0046

Ewart, A., Chappell, B. W., and Menzies, M. A. (1988). An Overview of the Geochemical and Isotopic Characteristics of the Eastern Australian CainozoicVolcanic Provinces. *J. Petrology* Special_Volume (1), 225–273. doi:10.1093/petrology/Special_Volume.1.225

Filippova, A., Frank, M., Kienast, M., Rickli, J., Hathorne, E., Yashayaev, I. M., et al. (2017). Water Mass Circulation and Weathering Inputs in the Labrador Sea Based on Coupled Hf-Nd Isotope Compositions and Rare Earth Element Distributions. *Geochimica Cosmochimica Acta* 199, 164–184. doi:10.1016/j.gca.2016.11.024

Fröllje, H., Pahnke, K., Schnetger, B., Brumsack, H.-J., Dulai, H., and Fitzsimmons, J. N. (2016). Hawaiian Imprint on Dissolved Nd and Ra Isotopes and Rare Earth Elements in the Central North Pacific: Local Survey and Seasonal Variability. *Geochimica Cosmochimica Acta* 189, 110–131. doi:10.1016/j.gca.2016.06.001

Ganachaud, A., Cravatte, S., Sprintall, J., Germineaud, C., Alberty, M., Jeandel, C., et al. (2017). The Solomon Sea: its Circulation, Chemistry, Geochemistry and Biology Explored during Two Oceanographic Cruises. *Elem. Sci. Anth* 5 (0), 33. doi:10.1525/elementa.221

Germineaud, C. (2016). *Circulation Océanique et Variabilité en Mer des Salomon*. (Doctoral thesis, Universite Toulouse 3 -Paul Sabatier). Retrieved from http://www.these.fr/.

Germineaud, C., Cravatte, S., Sprintall, J., Alberty, M. S., Grenier, M., and Ganachaud, A. (2021). Deep Pacific Circulation: New Insights on Pathways through the Solomon Sea. *Deep Sea Res. Part I Oceanogr. Res. Pap.* 171, 103510. doi:10.1016/j.dsr.2021.103510

Germineaud, C., Ganachaud, A., Sprintall, J., Cravatte, S., Eldin, G., Alberty, M. S., et al. (2016). Pathways and Water Mass Properties of the Thermocline and Intermediate Waters in the Solomon Sea. *J. Phys. Oceanogr.* 46 (10), 3031–3049. doi:10.1175/jpo-d-16-0107.1

Grenier, M., Cravatte, S., Blanke, B., Menkes, C., Koch-Larrouy, A., Durand, F., et al. (2011). From the Western Boundary Currents to the Pacific Equatorial Undercurrent: Modeled Pathways and Water Mass Evolutions. *J. Geophys. Res.* 116 (12), C12044. doi:10.1029/2011JC007477

Grenier, M., Jeandel, C., and Cravatte, S. (2014). From the Subtropics to the Equator in the Southwest Pacific: Continental Material Fluxes Quantified Using Neodymium Data along Modeled Thermocline Water Pathways. *J. Geophys. Res. Oceans* 119 (6), 3948–3966. doi:10.1002/2013JC009670

Grenier, M., Jeandel, C., Lacan, F., Vance, D., Venchiarutti, C., Cros, A., et al. (2013). From the Subtropics to the Central Equatorial Pacific Ocean: Neodymium Isotopic Composition and Rare Earth Element Concentration Variations. *J. Geophys. Res. Oceans* 118 (2), 592–618. doi:10.1029/2012JC008239

Grenier, M. (2012). Le role du Pacifique Tropical Sud-Ouest dans la Fertilisation DuPacifique Quatorial: Couplage Dynamique et Multi-Traceur. (Doctoral thesis, Universite Toulouse 3 -Paul Sabatier). Retrieved from http://www.these.fr/.

Handler, M. R., Bennett, V. C., and Carlson, R. W. (2005). Nd, Sr and Os Isotope Systematics in Young, Fertile Spinel Peridotite Xenoliths from Northern Queensland, Australia: A Unique View of Depleted MORB Mantle? *Geochimica Cosmochimica Acta* 69 (24), 5747–5763. doi:10.1016/j.gca.2005.08.003

Hegner, E., and Smith, I. E. M. (1992). Isotopic Compositions of Late Cenozoic Volcanics from Southeast Papua New Guinea: Evidence for Multi-Component Sources in Arc and Rift Environments. *Chem. Geol.* 97 (3–4), 233–249. doi:10.1016/0009-2541(92)90078-J

Homoky, W. B., John, S. G., Conway, T. M., and Mills, R. A. (2013). Distinct Iron Isotopic Signatures and Supply from Marine Sediment Dissolution. *Nat. Commun.* 4 (1), 1–10. doi:10.1038/ncomms3143

Homoky, W. B., Weber, T., Berelson, W. M., Conway, T. M., Henderson, G. M., van Hulten, M., et al. (2016). Quantifying Trace Element and Isotope Fluxes at the Ocean-Sediment Boundary: A Review, *Phil. Trans. R. Soc. A.* 374, 20160246. doi:10.1098/rsta.2016.0246

Jeandel, C., Arsouze, T., Lacan, F., Téchiné, P., and Dutay, J.-C. (2007). Isotopic Nd Compositions and Concentrations of the Lithogenic Inputs into the Ocean: A Compilation, with an Emphasis on the Margins. *Chem. Geol.* 239 (1–2), 156–164. doi:10.1016/j.chemgeo.2006.11.013

Jeandel, C. (1993). Concentration and Isotopic Composition of Nd in the South Atlantic Ocean. *Earth Planet. Sci. Lett.* 117 (3–4), 581–591. doi:10.1016/0012-821X(93)90104-H

Jeandel, C., and Derek, V. (2018). New Tools, New Discoveries in Marine Geochemistry. *Elements* 14 (6), 379–384. doi:10.2138/gselements.14.6.379

Jeandel, C., and Oelkers, E. H. (2015). The Influence of Terrigenous Particulate Material Dissolution on Ocean Chemistry and Global Element Cycles. *Chem. Geol.* 395, 50–66. doi:10.1016/j.chemgeo.2014.12.001

Jeandel, C. (2016). Overview of the Mechanisms that Could Explain the 'Boundary Exchange' at the Land-Ocean Contact. *Phil. Trans. R. Soc. A* 374, 20150287. doi:10.1098/rsta.2015.0287

Jeandel, C., Thouron, D., and Fieux, M. (1998). Concentrations and Isotopic Compositions of Neodymium in the Eastern Indian Ocean and Indonesian Straits. *Geochimica Cosmochimica Acta* 62 (15), 2597–2607. doi:10.1016/S0016-7037(98)00169-0

Johnson, K. S., Chavez, F. P., and Friederich, G. E. (1999). Continental-shelf Sediment as a Primary Source of Iron for Coastal Phytoplankton. *Nature* 398, 697–700. doi:10.1038/19511

Kamenetsky, V. S., Binns, R. A., Gemmell, J. B., Crawford, A. J., Mernagh, T. P., Maas, R., et al. (2001). Parental Basaltic Melts and Fluids in Eastern Manus Backarc Basin: Implications for Hydrothermal Mineralisation. *Earth Planet. Sci. Lett.* 184 (3–4), 685–702. doi:10.1016/S0012-821X(00)00352-6

Kawabe, M., and Fujio, S. (2010). Pacific Ocean Circulation Based on Observation. *J. Oceanogr.* 66 (3), 389–403. doi:10.1007/s10872-010-0034-8

Kessler, W. S., and Cravatte, S. (2013a). ENSO and Short-Term Variability of the South Equatorial Current Entering the Coral Sea. *J. Phys. Oceanogr.* 43, 956–969. doi:10.1175/JPO-D-12-0113.1

Kessler, W. S., and Cravatte, S. (2013b). Mean Circulation of the Coral Sea. *J. Geophys. Res. Oceans* 118, 6385–6410. doi:10.1002/2013JC009117

Labatut, M., Lacan, F., Pradoux, C., Chmeleff, J., Radic, A., Murray, J. W., et al. (2014). Iron Sources and Dissolved-Particulate Interactions in the Seawater of the Western Equatorial Pacific, Iron Isotope Perspectives. *Glob. Biogeochem. Cycles* 28, 1044–1065. doi:10.1002/2014GB004928

Lacan, F., and Jeandel, C. (2005). Neodymium Isotopes as a New Tool for Quantifying Exchange Fluxes at the Continent-Ocean Interface. *Earth Planet. Sci. Lett.* 232 (3–4), 245–257. doi:10.1016/j.epsl.2005.01.004

Lacan, F., and Jeandel, C. (2001). Tracing Papua New Guinea Imprint on the Central Equatorial Pacific Ocean Using Neodymium Isotopic Compositions and Rare Earth Element Patterns. *Earth Planet. Sci. Lett.* 186 (3–4), 497–512. doi:10.1016/S0012-821X(01)00263-1

Lambelet, M., Flierdt, T., Butler, E. C. V., Bowie, A. R., Rintoul, S. R., Watson, R. J., et al. (2018). The Neodymium Isotope Fingerprint of Adélie Coast Bottom Water. *Geophys. Res. Lett.* 45 (2011), 247256–247311. doi:10.1029/2018GL080074

Lindstrom, E., Lukas, R., Fine, R., Firing, E., Godfrey, S., Meyer, G., et al. (1987). The Western Equatorial Pacific Ocean Circulation Study. *Nature* 330, 533–537. doi:10.1038/330533a0

Lugmair, G. W., Scheinin, N. B., and Marti, K. (1975). Sm-Nd Age and History of Apollo 17 Basalt 75075: Evidence for Early Differentiation of the Lunar Exterior. *LPSC* 2, 1419–1429. Available at: https://ui.adsabs.harvard.edu/abs/1975LPSC....6.1419L/abstract.

McCartney, P. (1979). *Subantarctic Mode Water*. Woods Hole Ceanographic Institution Contribution 3773, 103–119.

Milliman, J. D. (1995). Sediment Discharge to the Ocean from Small Mountainous Rivers: The New Guinea Example. *Geo-Marine Lett.* 15 (3–4), 127–133. doi:10.1007/BF01204453

Milliman, J., Farnsworth, K., and Albertin, C. (1999). Flux and Fate of Fluvial Sediments Leaving Large Islands in the East Indies. *J. Sea Res.* 41, 97. doi:10.1016/s1385-1101(98)00040-9

Nohara, M., Hirose, K., Eissen, J. P., Urabe, T., and Joshima, M. (1994). The North Fiji Basin Basalts and Their Magma Sources: Part II. Sr-Nd Isotopic and Trace Element Constraints. *Mar. Geol.* 116 (1–2), 179–195. doi:10.1016/0025-3227(94)90175-9

Orsi, A. H., and Nowlin, W. D. (1995). On the Meridional Extent and Fronts of the Antarctic Circumpolar Current, 42 Deep Sea Research Part I: Oceanographic Research Papers. *Deep Sea Res. Part I Oceanogr. Res. Pap.* 42, 641. doi:10.1016/0967-0637(95)00021-W

Orsi, A. H., Johnson, G. C., and Bullister, J. L. (1999). Circulation, Mixing, and Production of Antarctic Bottom Water. *Prog. Oceanogr.* 43 (1), 55–109. doi:10.1016/S0079-6611(99)00004-X

Pham, V. Q., Grenier, M., Cravatte, S., Michael, S., Jacquet, S., Belhadj, M., et al. (2019). Dissolved Rare Earth Elements Distribution in the Solomon Sea. *Chem. Geol.* 524 (May), 11–36. doi:10.1016/j.chemgeo.2019.05.012

Pin, C., and Santos Zalduegui, J. F. (1997). Sequential Separation of Light Rare-Earth Elements, Thorium and Uranium by Miniaturized Extraction Chromatography: Application to Isotopic Analyses of Silicate Rocks. *Anal. Chim. Acta* 339 (1–2), 79–89. doi:10.1016/S0003-2670(96)00499-0

Pitchford, J., and Brindley, J. (1999). Iron Limitation, Grazing Pressure and Oceanic High Nutrient-Low Chlorophyll (HNLC) Regions. *J. Plankton Res.* 21 (3), 525–547. doi:10.1093/plankt/21.3.525

Qu, T., Gao, S., Fukumori, I., Fine, R. A., and Lindstrom, E. J. (2009). Origin and Pathway of Equatorial 13°C Water in the Pacific Identified by a Simulated Passive Tracer and its Adjoint*. *J. Phys. Oceanogr.* 39, 1836–1853. doi:10.1175/2009JPO4045.1

Qu, T., Gao, S., Fukumori, I., Fine, R. A., and Lindstrom, E. J. (2008). Subduction of South Pacific Waters. *Geophys. Res. Lett.* 35, L02610. doi:10.1029/2007GL032605

Qu, T., and Lindstrom, E. J. (2002). A Climatological Interpretation of the Circulation in the Western South Pacific. *J. Phys. Oceanogr.* 32 (9), 2492–2508. doi:10.1055/s-2007-989442

Radenac, M.-H., Léger, F., Singh, A., and Delcroix, T. (2012). Sea Surface Chlorophyll Signature in the Tropical Pacific during Eastern and Central Pacific ENSO Events. *J. Geophys. Res.* 117 (4), a–n. doi:10.1029/2011JC007841

Rahlf, P., Laukert, G., Hathorne, E. C., Vieira, L. H., and Frank, M. (2021). Dissolved Neodymium and Hafnium Isotopes and Rare Earth Elements in the Congo River Plume: Tracing and Quantifying Continental Inputs into the Southeast Atlantic. *Geochimica Cosmochimica Acta* 294, 192–214. doi:10.1016/j.gca.2020.11.017

Reid, J. L. (1997). On the Total Geostrophic Circulation of the Pacific Ocean: Flow Patterns, Tracers, and Transports. *Prog. Oceanogr.* 39 (4), 263–352. doi:10.1016/S0079-6611(97)00012-8

Robinson, S., Ivanovic, R., van de Flierdt, T., Blanchet, C. L., Tachikawa, K., Martin, E. E., et al. (2021). Global Continental and Marine Detrital ε_{Nd}: An Updated Compilation for Use in Understanding Marine Nd Cycling. *Chem. Geol.* 567, 120119. doi:10.1016/j.chemgeo.2021.120119

Rudnick, R. L., McDonough, W. F., McCulloch, M. T., and Taylor, S. R. (1986). Lower Crustal Xenoliths from Queensland, Australia: Evidence for Deep Crustal Assimilation and Fractionation of Continental Basalts. *Geochimica Cosmochimica Acta* 50 (6), 1099–1115. doi:10.1016/0016-7037(86)90391-1

Ryan, J. P., Ueki, I., Chao, Y., Zhang, H., Polito, P. S., and Chavez, F. P. (2006). Western Pacific Modulation of Large Phytoplankton Blooms in the Central and Eastern Equatorial Pacific. *J. Geophys. Res.* 111 (2), a–n. doi:10.1029/2005JG000084

Schuth, S., Münker, C., König, S., Qopoto, C., Basi, S., Garbe-Schönberg, D., et al. (2009). Petrogenesis of Lavas along the Solomon Island Arc, SW Pacific: Coupling of Compositional Variations and Subduction Zone Geometry. *J. Petrology* 50 (5), 781–811. doi:10.1093/petrology/egp019

Schuth, S., Rohrbach, A., Münker, C., Ballhaus, C., Garbe-Schönberg, D., and Qopoto, C. (2004). Geochemical Constraints on the Petrogenesis of Arc Picrites and Basalts, New Georgia Group, Solomon Islands. *Contrib. Mineral. Pet.* 148 (3), 288–304. doi:10.1007/s00410-004-0604-0

Shabani, M. B., Akagi, T., and Masuda, A. (1992). Preconcentration of Trace Rare-Earth Elements in Seawater by Complexation with Bis(2-Ethylhexyl) Hydrogen Phosphate and 2-Ethylhexyl Dihydrogen Phosphate Adsorbed on a C18 Cartridge and Determination by Inductively Coupled Plasma Mass Spectrometry. *Anal. Chem.* 64 (7), 737–743. doi:10.1021/ac00031a008

Sholkovitz, E. R. (1996). *A Compilation of the Rare Earth Element Composition of Rivers, Estuaries and the Oceans*. WHOI Tech- Nical Report, 72. *WHOI-96-13*(November).

Sholkovitz, E. R., Elderfield, H., Szymczak, R., and Casey, K. (1999). Island Weathering: River Sources of Rare Earth Elements to the Western Pacific Ocean. *Mar. Chem.* 68 (1–2), 39–57. doi:10.1016/S0304-4203(99)00064-X

Slemons, L. O., Murray, J. W., Resing, J., Paul, B., and Dutrieux, P. (2010). Western Pacific Coastal Sources of Iron, Manganese, and Aluminum to the Equatorial Undercurrent. *Glob. Biogeochem. Cycles* 24 (3), a–n. doi:10.1029/2009GB003693

Sokolov, S., and Rintoul, S. (2000). Circulation and Water Masses of the Southwest Pacific: WOCE Section P11, Papua New Guinea to Tasmania. *J. Mar. Res.* 58, 223–268. doi:10.1357/002224000321511151

Speckbacher, R., Behrmann, J., Nagel, T., Stipp, M., and Mahlke, J. (2012). Fluid Flow and Metasomatic Fault Weakening in the Moresby Seamount Detachment, Woodlark Basin, Offshore Papua New Guinea. *Geochem. Geophys. Geosyst.* 13 (11). doi:10.1029/2012GC004407

Stichel, T., Frank, M., Rickli, J., and Haley, B. A. (2012). The Hafnium and Neodymium Isotope Composition of Seawater in the Atlantic Sector of the Southern Ocean. *Earth Planet. Sci. Lett.* 317-318, 282–294. doi:10.1016/j.epsl.2011.11.025

Stichel, T., Hartman, A. E., Duggan, B., Goldstein, S. L., Scher, H., and Pahnke, K. (2015). Separating Biogeochemical Cycling of Neodymium from Water Mass Mixing in the Eastern North Atlantic. *Earth Planet. Sci. Lett.* 412, 245–260. doi:10.1016/j.epsl.2014.12.008

Stichel, T., Kretschmer, S., Geibert, W., Lambelet, M., Plancherel, Y., Rutgers Van Der Loeff, M., et al. (2020). Particle-Seawater Interaction of Neodymium in the North Atlantic. *ACS Earth Space Chem.* 4 (9), 1700–1717. doi:10.1021/acsearthspacechem.0c00034

Tachikawa, K., Jeandel, C., and Roy-Barman, M. (1999). A New Approach to the Nd Residence Time in the Ocean: the Role of Atmospheric Inputs. *Earth Planet. Sci. Lett.* 170 (4), 433–446. doi:10.1016/S0012-821X(99)00127-2

Takahashi, T., Olafsson, J., Goddard, J. G., Chipman, D. W., and Sutherland, S. C. (1993). Seasonal Variation of CO_2 and Nutrients in the High-Latitude Surface Oceans: A Comparative Study. *Glob. Biogeochem. Cycles* 7 (4), 843–878. doi:10.1029/93gb02263

Talley, L. D. (2007). *Hydrographic Atlas of the World Ocean Circulation Experiment (WOCE) Volume 2: Pacific Ocean*. Southampton: WOCE International Project Office.

Tomczak, M., and Godfrey, J. S. (2003). *Regional Oceanography: An Introduction*. 2nd ed. Newdelh, India: Daya Publishing House.

Tomczak, M., and Hao, D. (1989). Water Masses in the Thermocline of the Coral Sea. *Deep Sea Res. Part A. Oceanogr. Res. Pap.* 36 (10), 1503–1514. doi:10.1016/0198-0149(89)90054-X

Tsimplis, M. N., Bacon, S., and Bryden, H. L. (1998). The Circulation of the Subtropical South Pacific Derived from Hydrographic Data. *J. Geophys. Res. Oceans* 103 (C10), 21443–21468. doi:10.1029/98JC01881

Tsuchiya, M., Lukas, R., Fine, R. A., Firing, E., and Lindstrom, E. (1989). Source Waters of the Pacific Equatorial Undercurrent. *Prog. Oceanogr.* 23 (Issue 2), 101–147. doi:10.1016/0079-6611(89)90012-8

Tsuchiya, M. (1981). The Origin of the Pacific Equatorial 13°C Water. *J. Phys. Oceanogr.* 11 (6), 794–812. doi:10.1175/1520-0485(1981)011<0794:tootpe>2.0.co;2

Venables, H., and Moore, C. M. (2010). Phytoplankton and Light Limitation in the Southern Ocean: Learning from High-Nutrient, High-Chlorophyll Areas. *J. Geophys. Res.* 115 (C2), C02015. doi:10.1029/2009jc005361

Warren, B. A. (1973). Transpacific Hydrographic Sections at Lats. 43°S and 28°S: the SCORPIO Expedition—II. Deep Water. *Deep Sea Res. Oceanogr. Abstr.* 20 (1), 9–38. doi:10.1016/0011-7471(73)90040-5

Wilson, D. J., Piotrowski, A. M., Galy, A., and Clegg, J. A. (2013). Reactivity of Neodymium Carriers in Deep Sea Sediments: Implications for Boundary Exchange and Paleoceanography. *Geochimica Cosmochimica Acta* 109, 197–221. doi:10.1016/j.gca.2013.01.042

Zhang, M. (2001). Petrogenesis and Geodynamic Implications of Late Cenozoic Basalts in North Queensland, Australia: Trace-Element and Sr-Nd-Pb Isotope Evidence. *J. Petrology* 42 (4), 685–719. doi:10.1093/petrology/42.4.685

Conflict of Interest: The authors declare that the research was conducted in the absence of any commercial or financial relationships that could be construed as a potential conflict of interest.

Publisher's Note: All claims expressed in this article are solely those of the authors and do not necessarily represent those of their affiliated organizations, or those of the publisher, the editors and the reviewers. Any product that may be evaluated in this article, or claim that may be made by its manufacturer, is not guaranteed or endorsed by the publisher.